POLITECNICO DI TORINO
Repository ISTITUZIONALE

Energy, environmental and economic experimental assessment of a typical air-handling unit operating under single faults on valves, fans and sensors in south of Italy

Original
Energy, environmental and economic experimental assessment of a typical air-handling unit operating under single faults on valves, fans and sensors in south of Italy / Rosato, A., Youssef, M.E., Mercuri, R., Piscitelli, M.S., Capozzoli, A.. - In: ENERGY AND BUILDINGS. - ISSN 0378-7788. - 367:(2026). [10.1016/j.enbuild.2026.117746]

Availability:
This version is available at: 11583/3012755 since: 2026-07-06T11:02:14Z

Publisher:
Elsevier Ltd

Published
DOI:10.1016/j.enbuild.2026.117746

Terms of use:

This article is made available under terms and conditions as specified in the corresponding bibliographic description in the repository

Publisher copyright

(Article begins on next page)

15 November 2026

Energy & Buildings 367 (2026) 117746

Contents lists available at ScienceDirect

Energy & Buildings

journal homepage: www.elsevier.com/locate/enb

Energy, environmental and economic experimental assessment of a typical air-handling unit operating under single faults on valves, fans and sensors in south of Italy

Antonio Rosato [a,*], Mohammad El Youssef [a], Rita Mercuri [a], Marco Savino Piscitelli [b], Alfonso Capozzoli [b]

[a] Department of Architecture and Industrial Design, SENS i-Lab, University of Campania Luigi Vanvitelli, Via San Lorenzo 4, 81031 Aversa, Italy
[b] Department of Energy "Galileo Ferraris", Politecnico di Torino, Corso Duca degli Abruzzi 24, 10129 Turin, Italy

ARTICLE INFO

Keywords:
Air-handling unit
Valve stuck
Fan stuck
Offset of sensor
Faulty experimental data
Fault impact
Fault detection and diagnosis

ABSTRACT

Data-driven automated fault detection and diagnosis (AFDD) offers a significant advantage in optimizing AHU efficiency by enabling real-time fault detection. This study evaluates the field performance of a single-duct, dual-fan constant air volume AHU in a Mediterranean climate (southern Italy). The analysis considers both normal and faulty scenarios, including eleven commonly encountered faults (1) positive offset of the return air relative humidity sensor (+15%); 2) negative offset of the return air relative humidity sensor (–15%); 3) negative offset of the return air temperature sensor (–3 °C); 4) humidifier valve stuck at 0% (always closed); 5) positive offset of the return air temperature sensor (+3 °C); 6) cooling coil valve stuck at 100% (always open); 7) post-heating coil valve stuck at 0% (always closed); 8) post-heating coil valve stuck at 100% (always open); 9) cooling coil valve stuck at 0% (always closed); 10) complete failure of the return air fan; 11) complete failure of the supply air fan. The impact of these faults on AHU performance is assessed in terms of electrical power consumption, energy demand, operational costs, global equivalent CO_2 emissions as well as operation time. Among the investigated faults, experimental results highlight that the post-heating coil valve stuck at 100% significantly affects system performance; specifically, this fault decreases daily indoor air temperature met ratio by about 69% during summer and winter tests, while increases total daily electrical energy consumption, operational costs, and global equivalent CO_2 emissions by over than 60% during cooling period and by more than 80% during heating period. Through a comparative analysis between observed faulty data and normal performance under identical conditions, this study provides valuable insights for developing AFDD tools and assists building personnel in identifying symptoms of common AHU faults, thereby contributing to more efficient building management.

1. Introduction

It is known that building sector accounts for around 37% of global greenhouse gas (GHG) emissions and 36% of global final energy demand [1]. Heating, ventilation, and air conditioning (HVAC) systems account for 10 ÷ 20% of total energy consumption and 50 ÷ 60% of the energy demand of the building sector [2–4], making them strategically important for the achievement of EU targets in terms of energy savings [5]. HVAC systems, which often include Air-Handling Units (AHUs), are commonly run under faulty scenarios as a result of improper maintenance, component failure, or improper installation (according to [6,7]). AHU malfunctions might have serious consequences [8–10], including uncomfortable conditions for occupants, low indoor air quality, and large energy and financial losses. Automated Fault Detection and Diagnosis (AFDD) techniques can enable the automatic recognition of fault occurrence as well as identification/localization of problem sources [10]. Recommissioning AHUs to address malfunctioning operation via AFDD processes has been shown to result in an approximate 20 ÷ 30% reduction in energy consumption [11,12]. AFDD tools are divided into knowledge-based and data-driven categories by Zhao et al. [13]. Knowledge-driven approaches identify errors by analysing the patterns of certain variables and the similarities with pre-labelled anomaly libraries, whereas domain knowledge-based methods depend on physics rules. Recently the data-driven approach has garnered significant attention due to its potential for increasing accuracy and its applicability

* Corresponding author.
E-mail address: antonio.rosato@unicampania.it (A. Rosato).

https://doi.org/10.1016/j.enbuild.2026.117746
Received 27 October 2025; Received in revised form 29 December 2025; Accepted 1 June 2026
Available online 4 June 2026
0378-7788/© 2026 The Author(s). Published by Elsevier B.V. This is an open access article under the CC BY-NC-ND license (http://creativecommons.org/licenses/by-nc-nd/4.0/).

Nomenclature

Symbols

A	Current intensity (A)
AFDD	Automated fault detection and diagnosis
AHU	Air-handling unit
CAV	Constant air volume
CC	Cooling coil
cosθ	Power factor
CO_2	Carbon dioxide
CT	Cold tank
D	Damper
d	Deviation (°C, %)
DB	Deadband (°C, %)
EA	Exhaust air
E	Energy (kWh)
ETS	Experimental data acquisition time step
EXP	Experimental value
F	Filter
GHG	Global greenhouse gas
HP	Heat pump
HRS	Heat recovery system
HT	Hot tank
HUM	Humidifier
HVAC	Heating, ventilation and air-conditioning
KPI	Key performance index
L	Lower
MR	Met ratio (%)
m_x	Mass of a given pollutant (g)
mCO_2	Mass of global equivalent CO_2 emissions (gCO_2)
N	Number of experimental data points
OAD	Outdoor air duct
OC	Operating costs (€)
OL	Velocity percentage (%)
OP	Opening percentage (%)
OT	Operating time (min)
P	Power (W)
PHP	Circulating pump connected to the heat pump
PID	Proportional-integral-derivative
PostHC	Post-heating coil
PreHC	Pre-heating coil
PRS	Circulating pump connected to the refrigerating system
RAD	Return air duct
RAF	Return air fun
RH	Air relative humidity (%)
RHMR	Indoor air relative humidity met ratio (%)
RMSD	Root mean square difference (°C, %)
RS	Refrigerating system
SAD	Supply air duct
SAF	Supply air fan
SF1	Faulty test with a positive offset of the return air relative humidity sensor by + 15% during summer
SF2	Faulty test with a negative offset of the return air relative humidity sensor by –15% during summer
SF3	Faulty test with a positive offset of the return air temperature sensor by 3 °C during summer
SF4	Faulty test with the humidifier valve always kept closed during summer
SF5	Faulty test with a negative offset of the return air temperature sensor by –3 °C during summer
SF6	Faulty test with the cooling coil valve always kept open during summer
SF7	Faulty test with the post-heating coil valve always kept closed during summer
SF8	Faulty test with the post-heating coil valve always kept open during summer
SF9	Faulty test with the cooling coil valve always kept closed during summer
SF10	Faulty test with the complete failure of the return air fan during summer
SF11	Faulty test with the complete failure of the supply air fan during summer
SN1	Normal summer test n° 1
SN2	Normal summer test n° 2
SN3	Normal summer test n° 3
SN4	Normal summer test n° 4
SN5	Normal summer test n° 5
SN6	Normal summer test n° 6
T	Temperature (°C)
TMR	Indoor air temperature met ratio (%)
U	Upper
$U^{E_{el}}_{CO_2,i}$	Electric energy output-based emission factor (gCO_2/kWh)
$UC_{el,i}$	Energy output-based unit cost (€/MWh)
U_x	Energy output-based emission factor (g/kWh)
VAV	Variable air volume
V_{CC}	Three-way valve feeding the cooling coil
V_{HUM}	Three-way valve feeding the humidifier
V_{PostHC}	Three-way valve feeding the post-heating coil
V_{PreHC}	Three-way valve feeding the pre-heating coil
V	Voltage (V)
$\dot{V}$	Volumetric flow rate (m^3/h)
WF1	Faulty test with a positive offset of the return air relative humidity sensor by + 15% during winter
WF2	Faulty test with a negative offset of the return air relative humidity sensor by –15% during winter
WF3	Faulty test with a positive offset of the return air temperature sensor by 3 °C during winter
WF4	Faulty test with the humidifier valve always kept closed during winter
WF5	Faulty test with a negative offset of the return air temperature sensor by –3 °C during winter
WF6	Faulty test with the cooling coil valve always kept open during winter
WF7	Faulty test with the post-heating coil valve always kept closed during winter
WF8	Faulty test with the post-heating coil valve always kept open during winter
WF9	Faulty test with the cooling coil valve always kept closed during winter
WF10	Faulty test with the complete failure of the return air fan during winter
WF11	Faulty test with the complete failure of the supply air fan during winter
WN1	Normal winter test n° 1
WN2	Normal winter test n° 2
WN3	Normal winter test n° 3
WN4	Normal winter test n° 4
WN5	Normal winter test n° 5
WN6	Normal winter test n° 6
WN7	Normal winter test n° 7
WN8	Normal winter test n° 8
%d	Percentage difference (%)
%DTMR	Percentage difference in terms of indoor air temperature met ratio (%)
%DRHMR	Percentage difference in terms of indoor air relative humidity met ratio (%)
$\%E_{el}$	Percentage difference in terms of electrical energy demand (%)
$\%P_{el}$	Percentage difference in terms of electrical power demand

	(%)
$\%P_{el,max}$	Percentage difference in terms of maximum electrical power demand (%)
$\%CO_2$	Percentage difference in terms of the global equivalent CO_2 emissions (%)
%OT	Percentage difference in terms of operational time (%)
%OC	Percentage difference in terms of operational cost (%)
$\%V_{glycol}$	Percentage by volume of glycol in the heat carrier fluid (%)
$\%\delta(P_{el})$	Relative uncertainty of P_{el} (%)
$\%\mu_{el}$	Percentage difference in terms of electric power consumption arithmetic mean (%)
$\%\sigma_{el}$	Percentage difference in terms of electric power consumption standard deviation (%)
0	The fault causes not substantial changes (differences within ± 10%)
+	The fault causes slightly positive changes (differences between 10 and 20%)
+ +	The fault causes substantial positive changes (differences higher than 20%)
–	The fault causes slightly negative changes (differences between –10 and –20%)
– –	The fault causes substantial negative changes (differences lower than –20%)

Subscripts

A	Air
Baseline	Normal condition
CC	Cooling coil
CT	Cold tank
CO_2	Carbon dioxide
D	Damper
DB	Deadband (°C/%)
EA	Exhaust air
el	Electric
EXP	Experimental
F	Heat carrier fluid
Faulty	Faulty condition
HT	Hot tank
HP	Heat pump
HRS	Heat recovery system
HUM	Humidifier
i	Time step (s)
in	Inlet/ between upper and lower deadband
L	Phase
MA	Mixed air
max	Maximum
N	Final time step
OA	Outdoor air
out	Outlet/outside upper or lower deadband
PHP	Heat pump circulating pump
PostHC	Post-heating coil
PreHC	Pre-heating coil
PRS	Refrigerating system circulating pump
RA	Return air
RAF	Return air fan
RH	Relative humidity (%)
Room	Integrated test room
RS	Refrigerating system
SA	Supply air
SAF	Supply air fan
SP	Desired set-point
T	Temperature (°C)
tot	Total
V	Valve
x	Generic pollutant

Greeks

∞	AHU component has not been activated only during the normal test
Δ	Difference
δ	Uncertainty of the measured value (A, V, W)
ε_i	Instantaneous difference (°C, %)
$\overline{\varepsilon}$	Average error (°C, %)
$\lvert\overline{\varepsilon}\rvert$	Absolute average error (°C, %)
$\lvert\overline{\varepsilon}_{T,D}\rvert$	Relevance of deviations from desired indoor air temperatures (°C)
$\lvert\overline{\varepsilon}_{RH,D}\rvert$	Relevance of deviations from desired indoor air relative humidity (%)
μ_{el}	Arithmetic mean of electric power demand (W)
σ_{el}	Standard deviation of electric power demand (W)

in situations where physics-based operation is not fully defined [14,15]. However, data-driven AFDD tools are limited in their ability to extrapolate beyond the limits of their training datasets [14,15]. In this context, there is considerable promise in leveraging data analytics and artificial intelligence techniques [13,14].

1.1. Research gaps

Data-driven AFDD tools are acknowledged for their effectiveness in enhancing AHUs performance. However, literature emphasizes that these tools are yet in the early phases of adoption [12]. A number of research gaps remain to be addressed, notably the persistent lack of standardized datasets encompassing diverse operating scenarios, AHU setups, and equipment [12,16] for both developing new AFDD methods as well as evaluate the accuracy of existing AFDD tools. Therefore, the evolution of data-driven AFDD models necessitates the collection of reliable, scalable, and labelled datasets comprising normal and faulty data. However, these datasets are currently limited due to various factors [16–19]: (i) many AHUs lack the necessary sensors to measure key operational parameters comprehensively; (ii) obtaining faulty data is challenging due to the complexities and costs involved in implementing faults into real AHUs; (iii) fault effects are significantly influenced by boundary conditions, requiring analyses across broad operating conditions; (iv) similar symptoms can be associated with different fault types or severities, necessitating a significant number of accurate sensors; (v) technical expertise and field assessments are essential for accurately labelling the data; (vi) AHUs operate under transient conditions, experiencing variations in weather conditions and cooling/heating demands. These challenges underscore the complexities involved in gathering comprehensive and representative datasets for developing accurate and robust data-driven AFDD models.

The availability of such datasets for AHUs is limited. The literature review emphasizes the pressing need for additional efforts in obtaining new experimental faulty datasets to support the evolution and utilization of data-driven AFDD tools. This recognized scarcity is echoed by various authors. Lin et al. [12] stressed the necessity for additional public datasets that clearly characterize fault categories. Granderson et al. [20] highlighted the increasing demand for AHU faulty datasets to accurately evaluate AFDD tools. Granderson et al. [21] pointed out the rarity of open-access databases featured by validated ground-truth points. Casillas et al. [22] identified the lack of sufficient publicly shared datasets as one of the main obstacles in the development of AFDD methods. Hu et al. [23] concluded that additional research is crucial to acquire and share further experimental normal and faulty data of HVAC

units for the development of data-driven AFDD techniques. Presently, only five datasets with verified ground truth information regarding specific tagged faults are publicly accessible [21]. This scarcity poses a challenge for researchers and developers seeking comprehensive resources to test and assess the operation of different AFDD algorithms in the context of AHUs.

Moreover, these few datasets are characterized by some limitations. The field datasets available for data-driven AFDD techniques in AHUs have predominantly originated from American climatic conditions [19–21,24], with very few instances focusing on Mediterranean climates [25–27]. Notably, the sampling frequency of measurements significantly impacts the accuracy of AHU component performance representation; while the scientific literature suggests a minimum sampling rate of 35 s [28,29], most studies have adopted a 1-minute time interval [19,21,24–27]. Numerous data-driven AFDD tools have relied on the ASHRAE RP-1312 dataset [19], created in 2011 using a simulation model developed through HVACSIM + software [30]. This dataset was subsequently validated against data measured every 60 s during both normal and faulty operations under USA winter and summer weather conditions; it encompassed both dual-duct dual-fan and single-duct dual-fan variable air volume (VAV) AHUs.

Understanding how different faults and their severities impact various aspects is crucial for the advancement and practical application of AFDD tools. However, only a few experimental studies have quantitatively explored the impacts of faults on occupants' comfort, power demands, energy consumption, CO_2 emissions, and operating costs [12,16,20]. In particular, the need for environmental and economic analyses is mainly due to that the CO_2 equivalent emission factor and the unit costs of electricity in Italy, as in many other countries around the world, vary depending on the time of day [31]. Consequently, the occurrence of a fault, in addition to impacting energy consumption, also influences CO_2 equivalent emissions and operating costs in different ways depending on the time of day as well as the corresponding operation of the HVAC components. As a result, environmental and economic assessments could provide different and additional information compared to those derived exclusively from energy analysis. The importance of analysing operating costs with reference to the occurrence of faults in HVAC systems is also highlighted by [32]. This kind of comprehensive analyses is vital in shaping the future development and deployment of AFDD tools. For instance, Chen et al. [33] noted that many studies focused on fault impacts in terms of yearly energy demand, thermal/hygrometric comfort, or operational expenses in HVAC systems, but there's a need for additional research to quantitatively evaluate fault impacts on several key operating parameters. The literature review highlights the gaps in research concerning the effects of faults on AHU components, especially under Mediterranean climates and with lower sampling rates. There is a clear need for further experimental investigations to address these gaps comprehensively.

The scientific literature on AFDD tools underscores that several HVAC components frequently are characterized by operational issues during regular use. Granderson et al. [20] identified valves, fans, and sensors as the primary components in AHUs that may fail or provide incorrect signals. However, information regarding the frequency of fault occurrences in AHUs is limited due to the inconsistent availability of maintenance records with fault information [34]. Regarding specific components, Li and O'Neill [34] highlighted the significance of heating/cooling coils in AHU operation, noting that faults in related valves, such as valve stuck, can significantly reduce HVAC system efficiency; they [34] identified fouling, leaking, scaling, and stuck as the most common faults for heating/cooling coils. Dey et al. [35] assessed the probability of occurrence of 14 fault types linked with heating coils, cooling coils, air mixing boxes, controllers, and sensors according to one-year maintenance data of a VAV AHU serving a building at the University of Texas; they [35] found that return air damper stuck and heating coil valve leaking were the most frequent fault types.

There's limited scientific investigation concerning the experimental assessment of the impacts of humidifier's faults on AHU operation (also due to the fact that HVAC systems including the humidifier are not usual), while some studies have focused on heating and cooling coil valve faults. Granderson et al. [21] evaluated VAV and constant air volume (CAV) AHUs under different heating and cooling coil valve positions, but did not discuss the impacts related with these faults. Nehasil et al. [36] experimentally validated an AFDD method for detecting faults in heating and cooling coil valves in a CAV AHU. Wen and Li [19] explored the effects of cooling coil valve faults in a VAV AHU during different seasons. Feng et al. [37] studied an AFDD method's performance with cooling coil valve faults in a VAV AHU during summer. Carling [38] compared three AFDD methods in an AHU with cooling coil valve faults under cooling mode in Stockholm (Sweden). These studies underscore the significance of various faults in AHU components, particularly valves associated with heating and cooling coils, and highlight the ongoing efforts to develop effective AFDD methods for detecting and addressing these faults in HVAC systems. The literature review emphasizes that studies on valves, especially regarding humidifier, are limited in number and have not been conducted in Mediterranean climates. Additionally, some studies were performed only in a single season, and the data acquisition frequency of field data was not less than 1 min. This lack of research emphasizes the necessity for new experimental studies to comprehensively investigate the impacts of such faults on typical AHU operations. Various studies indicate that sensors, actuators, and fans are common components in AHUs that experience failures or provide erroneous signals. Studies on sensor offsets, particularly related to return/indoor air temperature sensors, are limited in number and haven't covered Mediterranean climates extensively.

1.2. Novelty, goals and structure of the paper

In this study the experimental setup of the SENS i-Lab at the University of Campania Luigi Vanvitelli (Aversa, south Italy) [39] is exploited. This setup consists of an HVAC system equipped with a single-duct dual-fan CAV AHU fully designed and instrumented for AFDD purposes. In particular, this unit is equipped with a specifically developed control system permitting the users to artificially simulate the occurrence of predefined faults at different severity levels. In this study, reliable and high-quality monitoring datasets representing both normal and faulty tests during both cooling and heating seasons of the above-mentioned AHU are presented and analysed. Data have been measured every 1-second during 9-hour daily field tests running from 9 a.m. up to 6 p.m.

In more detail, the following 11 typical faults' types and severities have been experimentally studied: 1) positive offset of the return air relative humidity sensor readings by +15%; 2) negative offset of the return air relative humidity sensor readings by –15%; 3) humidifier valve stuck at 0% (always kept totally closed); 4) positive offset of the return air temperature sensor readings by +3 °C; 5) negative offset of the return air temperature sensor readings by –3 °C; 6) cooling coil valve stuck at 100% (always kept fully open); 7) cooling coil valve stuck at 0% (always kept totally closed); 8) post-heating coil valve stuck at 100% (always kept fully open); 9) post-heating coil valve stuck at 0% (always totally closed); 10) complete failure of the return air fan; 11) complete failure of the supply air fan.

This paper analyses the impacts of 11 aforementioned faults in terms of (i) power demand, (ii) electric energy consumption, (iii) operating costs, (vi) global equivalent CO_2 emissions, and (v) operational time. Previous studies [40,41] focused on the impacts of such faults in terms of thermo-hygrometric comfort as well as key operating parameters' patterns. This study mainly aims at: (i) underscoring the differences between AHU faulty operation and its nominal normal performance; (ii) evaluating the energy, environmental and economic impacts of the selected faults; (iii) identifying AHU faults with the most significant effects to prioritize future maintenance programs; (iv) developing a reliable dataset of faulty and normal operations of a typical AHU

operating under Italian weather conditions to support the future development of data-driven AFDD methods and evaluate the accuracy of existing AFDD tools.

This study deals with the key barriers towards a wider development and implementation of data-driven AFDD tools in AHUs by addressing the main following research gaps:

- limitation of field normal and faulty AHU datasets with verified ground truth information;
- field AHU databases predominantly originated under American climatic conditions, with very few instances focusing on Mediterranean climates;
- most data obtained with a 1-minute time interval;
- assessment of AHU faults' impacts mainly performed from an energy point of view only;
- very rare scientific investigation concerning AHU configurations including the humidifier (the operation of the humidification system is almost entirely absent from publicly available fault datasets, despite its relevance in terms of energy consumption, indoor air quality, and seasonal variability);
- few studies focusing on the impacts of faults associated to AHU humidifier.

Quantifying the energy, environmental and economic impacts of AHU faults is really valuable for multiple stakeholders. For facility managers, it enables informed prioritization of maintenance actions based on the actual consequences of faults. It also helps justify investments in diagnostic tools by linking fault persistence to increased operational costs, equipment degradation, and comfort risks. For policymakers, such kind of quantification provides the necessary evidence to shape performance-oriented regulation. With reference to this point, an example is the Smart Readiness Indicator (SRI) [42], which includes AFDD as a functional service contributing to building smartness. However, the current formulation of the SRI remains largely generic, without specifying the diagnostic depth or coverage required to address particular fault types. Without quantitative data on fault impacts, tools may be rated based on nominal availability rather than actual effectiveness, limiting the regulatory push toward meaningful deployment. System designers also benefit from this information, as it helps in identifying which faults have the highest operational relevance, allowing for more targeted design of resilient and maintainable systems. In particular, understanding fault impacts makes designers more sensitive to the role of the monitoring infrastructure, which must provide the necessary data granularity and reliability to enable advanced AFDD capabilities. This awareness supports a shift from compliance-based design toward performance-driven approaches, where diagnostics are not treated as add-ons but as core functions embedded in the building automation framework.

This paper consists of six main sections. Section 2 provides detailed information about the experimental setup, reporting the characteristics of AHU components, sensors and management system. Section 3 explains the methodology and the experiment design. Section 4 describes the boundary conditions of both the normal and faulty experiments by comparing them in terms of outside air temperature and relative humidity. Section 5 presents the results and discusses the experimental data and the outcomes of the assessment of faults' impact on system performance. The last section 6 summarizes the findings and outlines the future research directions.

2. Description of the experimental set-up

In this section, the experimental set-up is described in detail in terms of HVAC system and test room it serves (subsection 2.1), sensors used along with their measurement ranges and uncertainties (subsection 2.2), and logics governing the HVAC system operation (subsection 2.3).

2.1. HVAC system

A conventional HVAC system, including a single-duct dual-fan CAV AHU, serves the test room located in the SENS i-Lab of the Department of Architecture and Industrial Design at the University of Campania Luigi Vanvitelli (Aversa, southern Italy) [39]. The AHU under investigation is consistent with actual systems used in real applications. The test room has a floor area of 4.0 m × 4.0 m with a height of 3.6 m; it features four vertical walls (including one door, but no windows), as well as a horizontal ceiling and a horizontal floor. Fig. 1 presents the schematic of the HVAC system, while the details regarding the characteristics of its main components are provided in Table 1. In particular, two fans (manufactured by ZIEHL-ABEGG company) are installed in the AHU, the first one (named Supply Air Fan (SAF)) supplies air to the test room, while the other one (named Return Air Fan (RAF)) extracts air from the test room. The SAF is the model RH31C-ZID [43] (type: GR31C-ZID.DC.CR, article number: 14535/*H*01), with a diameter of 450 mm and a thickness equal to 318 mm. This fan is a three-phase alternating current system, delivering a nominal airflow rate of 600 m^3/h with a nominal power demand equal to 2.5 kW; it has a nominal pressure drop of 105 Pa, together with a motor efficiency of 26.1% as well as a sound pressure level equal to 90 dB. The RAF is the model RH25C-6ID [44] (type: GR25C-6ID.BD.CR, article number: 114855/*H*01), with a diameter of 375 mm and a thickness equal to 270 mm; it is a single-phase alternating current system, delivering a nominal airflow rate of 600 m^3/h with a nominal power consumption equal to 0.5 kW. It has a nominal pressure drop of 149 Pa, together with a motor efficiency of 41.5% as well as a sound pressure level equal to 78 dB. As reported in Fig. 1 and Table 1, the AHU is equipped with three coils, but the pre-heating coil (PreHC) is not used during the tests. The post-heating coil (PostHC) has a nominal heating capacity of 5.0 kW, a nominal airflow rate of 600 m^3/h (with a nominal pressure drop of 4.97 Pa) and a nominal water flowrate of 0.871 m^3/h (with a nominal pressure drop of 20.35 Pa); the cooling coil (CC) is characterized by a nominal cooling capacity of 5.0 kW, a nominal airflow rate of 600 m^3/h (with a nominal pressure drop of 17.80 Pa) and a nominal water flowrate of 0.857 m^3/h (with a nominal pressure drop of 13.56 Pa). The cold/hot heat transfer fluid is a water-ethylene glycol mixture (approximately 6% by volume of ethylene glycol), which is circulated by the pump PRS between the electric air-to-water vapor compression refrigerating system (RS) and the CC, as well as by the pump PHP between the electric air-to-water vapor compression heat pump (HP) and the PostHC. In addition, the AHU is equipped with a humidifier (HUM) manufactured by the company CAREL INDUSTRIES S.p.A. The HUM model (UE005X [45]) a three-phase alternating current system and has a nominal power rating of 3.7 kW, with a nominal steam production capacity of 5 kg/h.

2.2. Sensors and measurement uncertainty

The AHU is equipped with accurate sensors intended to monitor and record the temporal patterns of its most important operating parameters via a control panel developed within LabVIEW environment [47]. Taking into account that specifying the measurement accuracy is crucial for quantifying the reliability of test data [48], Table 2 presents both the measuring range and accuracy of all sensors. In particular, the experimental set-up is equipped with a duct return air sensor (model QFM2160 [49], manufactured by Siemens) allowing to measure both return air temperature (T_{RA}) and return air relative humidity (RH_{RA}) in order to control indoor conditions and regulate the AHU operation. In the test room, there are four air grilles (each 0.08 × 0.18 cm^2) mounted on the vertical walls at floor level (distributed at the four corners of the room) to extract air from the indoor environment; each grille is connected to a separate return duct, and these four ducts are collectively connected to the main return air duct. The above-mentioned return air sensor is installed inside the main return air duct.

The following equations are used to calculate the electric power

CC: cooling coil; CT: cold tank; D_{HRS}: heat recovery system dumper; D_{OA}: outdoor air dumper; D_{RA}: return air dumper; D_{EA}: exhaust air dumper; F_{OA}: outdoor air filter; F_{RA}: return air filter; F_{SA}: supply air filter; HRS: heat recovery system; HP: heat pump; HT: hot tank; HUM: humidifier; OAD: outdoor air duct; PreHC: pre-heating coil; PostHC: post-heating coil; PHP: circulating pump of heat pump; PRS: circulating pump of refrigerating system; RAD: return air duct; RAF: return air fan; RS: refrigerating system; SAD: supply air duct; SAF: supply air fan.

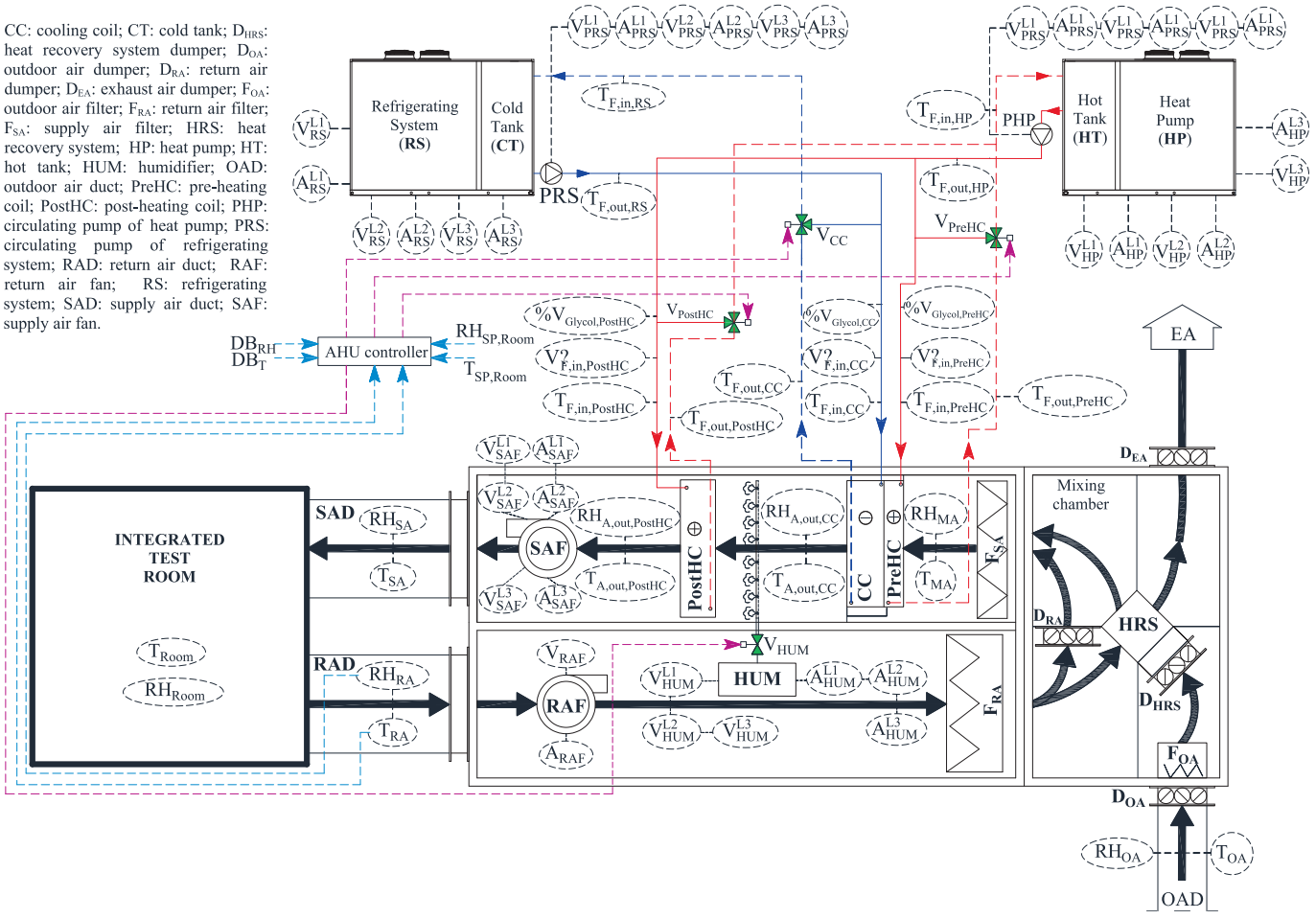


Fig. 1. Operating scheme of the HVAC system.

Table 1
Main nominal characteristics of the HVAC system major components.

Supply air fan [43]	Nominal supply air flow rate (m^3/h)	600
	Nominal power (kW)	2.50
Return air fan [44]	Nominal return air flow rate (m^3/h)	600
	Nominal power (kW)	0.50
Cross flow heat recovery system (HRS)	Nominal efficiency (%)	74.7
	Recovery capacity (kW)	3.1
Pre-heating coil	Nominal heating capacity (kW)	4.1
	Nominal heat carrier fluid flow rate (m^3/h)	0.71
	Nominal air flow rate (m^3/h)	600
Cooling coil	Nominal cooling capacity (kW)	5.0
	Nominal heat carrier fluid flow rate (m^3/h)	0.86
	Nominal air flow rate (m^3/h)	600
Humidifier [45]	Nominal steam capacity (kg/h)	5.0
	Nominal power (kW)	3.7
Post-heating coil	Nominal heating capacity (kW)	5.0
	Nominal heat carrier fluid flow rate (m^3/h)	0.86
	Nominal air flow rate (m^3/h)	600
Heat pump [46]	Nominal heating capacity (kW)	13.8
	Nominal input power (compressor and evaporator fan) (kW)	4.5
Refrigerating system [46]	Nominal cooling capacity (kW)	13.6
	Nominal input power (compressor and condenser fan) (kW)	4.2

demand (P_{el}) of (i) the SAF ($P_{el,SAF}$), (ii) the RAF ($P_{el,RAF}$), (iii) the HP ($P_{el,HP}$), (iv) the PHP ($P_{el,PHP}$), (v) the RS ($P_{el,RS}$), (vi) the PRS ($P_{el,PRS}$) as well as (vii) the HUM ($P_{el,HUM}$) according to the measured values of current intensity and voltage:

$$P_{el,SAF} = \frac{\left(V_{SAF}^{L1} \cdot A_{SAF}^{L1} + V_{SAF}^{L2} \cdot A_{SAF}^{L2} + V_{SAF}^{L3} \cdot A_{SAF}^{L3}\right) \cdot \cos\varphi_{SAF}}{\sqrt{3}} \quad (1)$$

$$P_{el,RAF} = V_{RAF} \cdot A_{RAF} \cdot \cos\varphi_{RAF} \quad (2)$$

$$P_{el,HP} = \left(V_{HP}^{L1} \cdot A_{HP}^{L1} + V_{HP}^{L2} \cdot A_{HP}^{L2} + V_{HP}^{L3} \cdot A_{HP}^{L3}\right) \cdot \cos\varphi_{HP} \quad (3)$$

$$P_{el,PHP} = \left(V_{PHP}^{L1} \cdot A_{PHP}^{L1} + V_{PHP}^{L2} \cdot A_{PHP}^{L2} + V_{PHP}^{L3} \cdot A_{PHP}^{L3}\right) \cdot \cos\varphi_{PHP} \quad (4)$$

Table 2
Main characteristics of sensors.

Measured parameter	Measuring range	Accuracy
Return air temperature T_{RA} [49] Supply air temperature T_{SA} [49] Mixed air temperature T_{MA} [49] Air temperature at the outlet of the CC $T_{A,out,CC}$ [49] Air temperature at the outlet of the PostHC $T_{A,out,PostHC}$ [49]	0 ÷ 50 °C	±0.8 °C (between 15 °C and 35 °C); ±1 °C (between 0 °C and 50 °C),
Outdoor air temperature T_{OA} [50]	–40 ÷ 60 °C	±0.2 °C at T_{OA} = 20 °C;±(–0.008333 · T_{OA} + 0.366667) °C when T_{OA} < 20 °C;±(0.00875 · T_{OA} – 0.025) °C when T_{OA} > 20 °C
Indoor air temperature T_{Room} [51]	–10 ÷ 60 °C	±0.5 °C at 25 °C + 0.03 °C/°C
Temperature of the heat carrier fluid at the outlet of the HP $T_{F,out,HP}$ [52] Temperature of the heat carrier fluid at the inlet of the HP $T_{F,in,HP}$ [52] Temperature of the heat carrier fluid at the outlet of the RS $T_{F,out,RS}$ [52] Temperature of the heat carrier fluid at the inlet of the RS $T_{F,in,RS}$ [52]	–10 ÷ 60 °C	±(0.03 + 0.0005 · T_F) °C
Temperature of the heat carrier fluid at the outlet of the PreHC $T_{F,out,PreHC}$ [53] Temperature of the heat carrier fluid at the inlet of the PreHC $T_{F,in,PreHC}$ [53] Temperature of the heat carrier fluid at the outlet of the PostHC $T_{F,out,PostHC}$ [53] Temperature of the heat carrier fluid at the inlet of the PostHC $T_{F,in,PostHC}$ [53] Temperature of the heat carrier fluid at the outlet of the CC $T_{F,out,CC}$ [53] Temperature of the heat carrier fluid at the inlet of the CC $T_{F,in,CC}$ [53]	–10 ÷ 120 °C	±0.6 °C at 60 °C
Return air relative humidity RH_{RA} [49] Supply air relative humidity RH_{SA} [49] Mixed air relative humidity RH_{MA} [49] Air relative humidity at the outlet of the CC $RH_{A,out,CC}$ [49] Air relative humidity at the outlet of the PostHC $RH_{A,out,PostHC}$ [49]	0 ÷ 100%	±3% (between 30% and 70%);±5% (between 0% and 100%)
Outdoor air relative humidity RH_{OA} [50]	0 ÷ 100%	±(2.3 + 0.008 of reading) %
Indoor air relative humidity RH_{Room} [51]	0 ÷ 95%	±3% at 25 °C + 0.2%/°C
Volumetric flow rate of the heat carrier fluid passing through the PreHC $\dot{V}_{F.in.PreHC}$ [53] Volumetric flow rate of the heat carrier fluid passing through the CC $\dot{V}_{F.in.CC}$ [53] Volumetric flow rate of the heat carrier fluid passing through the PostHC $\dot{V}_{F.in.PostHC}$ [53]	0.70 ÷ 2.34 m^3/h	±2% at 20 °C with % V_{glycol} = 0%
HP single phase L1 voltage V_{HP}^{L1} [54] HP single phase L2 voltage V_{HP}^{L2} [54] HP single phase L3 voltage V_{HP}^{L3} [54] RS single phase L1 voltage V_{RS}^{L1} [54] RS single phase L2 voltage V_{RS}^{L2} [54] RS single phase L3 voltage V_{RS}^{L3} [54] SAF single phase L1voltag V_{SAF}^{L1} [54] SAF single phase L2 voltage V_{SAF}^{L2} [54] SAF single phase L3 voltage V_{SAF}^{L3} [54] HUM single phase L1voltage V_{HUM}^{L1} [54] HUM single phase L2 voltage V_{HUM}^{L2} [54] HUM single phase L3 voltage V_{HUM}^{L3} [54] PHP single phase L1 voltage V_{PHP}^{L1} [54] PHP single phase L2 voltage V_{PHP}^{L2} [54] PHP single phase L3 voltage V_{PHP}^{L3} [54] PRS single phase L1 voltage V_{PRS}^{L1} [54] PRS single phase L2 voltage V_{PRS}^{L2} [54] PRS single phase L3 voltage V_{PRS}^{L3} [54]	0 ÷ 425 V	±0.50% of full scale
RAF voltage V_{RAF} [54]	0 ÷ 280 V	±0.50% of full scale
SAF single phase L1 current A_{SAF}^{L1} [54] SAF single phase L2 current A_{SAF}^{L2} [54] SAF single phase L3 current A_{SAF}^{L3} [54] HUM single phase L1 current A_{HUM}^{L1} [54] HUM single phase L2 current A_{HUM}^{L2} [54] HUM single phase L3 current A_{HUM}^{L3} [54]	0 ÷ 12.5 A	±0.50% of full scale
HP single phase L1 current A_{HP}^{L1} [54] HP single phase L2 current A_{HP}^{L2} [54] HP single phase L3 current A_{HP}^{L3} [54] RS single phase L1 current A_{RS}^{L1} [54] RS single phase L2 current A_{RS}^{L2} [54] RS single phase L3 current A_{RS}^{L3} [54] PHP single phase L1 current A_{PHP}^{L1} [54] PHP single phase L2 current A_{PHP}^{L2} [54] PHP single phase L3 current A_{PHP}^{L3} [54] PRS single phase L1 current A_{PRS}^{L1} [54] PRS single phase L2 current A_{PRS}^{L2} [54] PRS single phase L3 current A_{PRS}^{L3} [54]	0 ÷ 50 A	±0.50% of full scale
RAF current A_{RAF} [54]	0 ÷ 2.5 A	±0.50% of full scale

$$P_{el,RS} = \left(V_{RS}^{L1} \cdot A_{RS}^{L1} + V_{RS}^{L2} \cdot A_{RS}^{L2} + V_{RS}^{L3} \cdot A_{RS}^{L3}\right) \cdot \cos\varphi_{RS} \quad (5)$$

$$P_{el,PRS} = \left(V_{PRS}^{L1} \cdot A_{PRS}^{L1} + V_{PRS}^{L2} \cdot A_{PRS}^{L2} + V_{PRS}^{L3} \cdot A_{PRS}^{L3}\right) \cdot \cos\varphi_{PRS} \quad (6)$$

$$P_{el,HUM} = \frac{\left(V_{HUM}^{L1} \cdot A_{HUM}^{L1} + V_{HUM}^{L2} \cdot A_{HUM}^{L2} + V_{HUM}^{L3} \cdot A_{HUM}^{L3}\right) \cdot \cos\varphi_{HUM}}{\sqrt{3}} \quad (7)$$

where $\cos\varphi_{SAF}$, $\cos\varphi_{RAF}$, $\cos\varphi_{HP}$, $\cos\varphi_{PHP}$, $\cos\varphi_{RS}$, $\cos\varphi_{PRS}$ and $\cos\varphi_{HUM}$ are the power factors of the SAF, the RAF, the HP, the PHP, the RS, the PRS and the HUM, respectively. The following values suggested by the manufacturers have been assumed for the power factors: $\cos\varphi_{SAF} = 0.95$, $\cos\varphi_{RAF} = 0.95$, $\cos\varphi_{HP} = 0.95$, $\cos\varphi_{PHP} = 0.95$, $\cos\varphi_{RS} = 0.95$, $\cos\varphi_{PRS} = 0.95$, and $\cos\varphi_{HUM} = 0.95$.

The absolute measurement errors $\delta(P_{el,SAF})$, $\delta(P_{el,RAF})$, $\delta(P_{el,HP})$, $\delta(P_{el,PHP})$, $\delta(P_{el,RS})$, $\delta(P_{el,PRS})$ and $\delta(P_{el,HUM})$ associated to the evaluation of power consumption of the SAF (Eq. (1), the RAF (Eq. (2), the HP (Eq. (3), the PHP (Eq. (4), the RS (Eq. (5), the PRS (Eq. (6) as well as the HUM (Eq. (7), respectively, can be derived according to the single-sample uncertainty analysis suggested by Moffat [55] by means of the following equations:

$$\delta(P_{el,SAF}) = \left(\frac{\cos\varphi_{SAF}}{\sqrt{3}}\right)\cdot\sqrt{\begin{array}{c}\left[A_{SAF}^{L1}\cdot\delta\left(V_{SAF}^{L1}\right)\right]^2+\left[V_{SAF}^{L1}\cdot\delta\left(A_{SAF}^{L1}\right)\right]^2+\left[A_{SAF}^{L2}\cdot\delta\left(V_{SAF}^{L2}\right)\right]^2+\\ \left[V_{SAF}^{L2}\cdot\delta\left(A_{SAF}^{L2}\right)\right]^2+\left[A_{SAF}^{L3}\cdot\delta\left(V_{SAF}^{L3}\right)\right]^2+\left[V_{SAF}^{L3}\cdot\delta\left(A_{SAF}^{L3}\right)\right]^2\end{array}} \quad (8)$$

$$\delta(P_{el,RAF}) = (\cos\varphi_{RAF})\cdot\sqrt{\left[A_{RAF}\cdot\delta(V_{RAF})\right]^2+\left[V_{RAF}\cdot\delta(A_{RAF})\right]^2} \quad (9)$$

$$\delta(P_{el,HP}) = (\cos\varphi_{HP})\cdot\sqrt{\begin{array}{c}\left[A_{HP}^{L1}\cdot\delta\left(V_{HP}^{L1}\right)\right]^2+\left[V_{HP}^{L1}\cdot\delta\left(A_{HP}^{L1}\right)\right]^2+\left[A_{HP}^{L2}\cdot\delta\left(V_{HP}^{L2}\right)\right]^2+\\ \left[V_{HP}^{L2}\cdot\delta\left(A_{HP}^{L2}\right)\right]^2+\left[A_{HP}^{L3}\cdot\delta\left(V_{HP}^{L3}\right)\right]^2+\left[V_{HP}^{L3}\cdot\delta\left(A_{HP}^{L3}\right)\right]^2\end{array}} \quad (10)$$

$$\delta(P_{el,PHP}) = (\cos\varphi_{PHP})\cdot\sqrt{\begin{array}{c}\left[A_{PHP}^{L1}\cdot\delta\left(V_{PHP}^{L1}\right)\right]^2+\left[V_{PHP}^{L1}\cdot\delta\left(A_{PHP}^{L1}\right)\right]^2+\left[A_{PHP}^{L2}\cdot\delta\left(V_{PHP}^{L2}\right)\right]^2+\\ \left[V_{PHP}^{L2}\cdot\delta\left(A_{PHP}^{L2}\right)\right]^2+\left[A_{PHP}^{L3}\cdot\delta\left(V_{PHP}^{L3}\right)\right]^2+\left[V_{PHP}^{L3}\cdot\delta\left(A_{PHP}^{L3}\right)\right]^2\end{array}} \quad (11)$$

$$\delta(P_{el,RS}) = (\cos\varphi_{RS})\cdot\sqrt{\begin{array}{c}\left[A_{RS}^{L1}\cdot\delta\left(V_{RS}^{L1}\right)\right]^2+\left[V_{RS}^{L1}\cdot\delta\left(A_{RS}^{L1}\right)\right]^2+\left[A_{RS}^{L2}\cdot\delta\left(V_{RS}^{L2}\right)\right]^2+\\ \left[V_{RS}^{L2}\cdot\delta\left(A_{RS}^{L2}\right)\right]^2+\left[A_{RS}^{L3}\cdot\delta\left(V_{RS}^{L3}\right)\right]^2+\left[V_{RS}^{L3}\cdot\delta\left(A_{RS}^{L3}\right)\right]^2\end{array}} \quad (12)$$

$$\delta(P_{el,PRS}) = (\cos\varphi_{PRS})\cdot\sqrt{\begin{array}{c}\left[A_{PRS}^{L1}\cdot\delta\left(V_{PRS}^{L1}\right)\right]^2+\left[V_{PRS}^{L1}\cdot\delta\left(A_{PRS}^{L1}\right)\right]^2+\left[A_{PRS}^{L2}\cdot\delta\left(V_{PRS}^{L2}\right)\right]^2+\\ \left[V_{PRS}^{L2}\cdot\delta\left(A_{PRS}^{L2}\right)\right]^2+\left[A_{PRS}^{L3}\cdot\delta\left(V_{PRS}^{L3}\right)\right]^2+\left[V_{PRS}^{L3}\cdot\delta\left(A_{PRS}^{L3}\right)\right]^2\end{array}} \quad (13)$$

$$\delta(P_{el,HUM}) = \left(\frac{\cos\varphi_{HUM}}{\sqrt{3}}\right)\cdot\sqrt{\begin{array}{c}\left[A_{HUM}^{L1}\cdot\delta\left(V_{HUM}^{L1}\right)\right]^2+\left[V_{HUM}^{L1}\cdot\delta\left(A_{HUM}^{L1}\right)\right]^2+\left[A_{HUM}^{L2}\cdot\delta\left(V_{HUM}^{L2}\right)\right]^2+\\ \left[V_{HUM}^{L2}\cdot\delta\left(A_{HUM}^{L2}\right)\right]^2+\left[A_{HUM}^{L3}\cdot\delta\left(V_{HUM}^{L3}\right)\right]^2+\left[V_{HUM}^{L3}\cdot\delta\left(A_{HUM}^{L3}\right)\right]^2\end{array}} \quad (14)$$

where $\delta(V_{SAF}^{L1})$, $\delta(A_{SAF}^{L1})$, $\delta(V_{SAF}^{L2})$, $\delta(A_{SAF}^{L2})$,$\delta(V_{SAF}^{L3})$, $\delta(A_{SAF}^{L3})$, $\delta(V_{RAF})$, $\delta(A_{RAF})$, $\delta(V_{HP}^{L1})$, $\delta(A_{HP}^{L1})$, $\delta(V_{HP}^{L2})$, $\delta(A_{HP}^{L2})$, $\delta(V_{HP}^{L3})$, $\delta(A_{HP}^{L3})$, $\delta(V_{PHP}^{L1})$, $\delta(A_{PHP}^{L1})$, $\delta(V_{PHP}^{L2})$, $\delta(A_{PHP}^{L2})$, $\delta(V_{PHP}^{L3})$, $\delta(A_{PHP}^{L3})$,$\delta(V_{RS}^{L1})$, $\delta(A_{RS}^{L1})$, $\delta(V_{RS}^{L2})$, $\delta(A_{RS}^{L2})$, $\delta(V_{RS}^{L3})$, $\delta(A_{RS}^{L3})$, $\delta(V_{PRS}^{L1})$, $\delta(A_{PRS}^{L1})$, $\delta(V_{PRS}^{L2})$, $\delta(A_{PRS}^{L2})$, $\delta(V_{PRS}^{L3})$, $\delta(A_{PRS}^{L3})$, $\delta(V_{HUM}^{L1})$, $\delta(A_{HUM}^{L1})$, $\delta(V_{HUM}^{L2})$, $\delta(A_{HUM}^{L2})$, $\delta(V_{HUM}^{L3})$, and $\delta(A_{HUM}^{L3})$ represent the uncertainties (indicated in Table 2) associated to the measurement of voltage and current intensity of the SAF, RAF, HP, PHP,RS, PRS and HUM.

The relative uncertainties $\%\delta(P_{el,i})$ of $\delta(P_{el,SAF})$, $\delta(P_{el,RAF})$, $\delta(P_{el,HP})$, $\delta(P_{el,PHP})$, $\delta(P_{el,RS})$, $\delta(P_{el,PRS})$ and $\delta(P_{el,HUM})$ can be calculated as the ratios between the values of uncertainties (derived from Eqs. 8–14) and the actual measured power values $P_{el,i}$ at i-th time step according to (Eq. (15):

$$\%\delta(P_{el,i}) = \frac{\delta(P_{el,i})}{P_{el,i}}\cdot 100 \quad (15)$$

2.3. Control logics of the AHU

The operation of the HVAC system is controlled through a dedicated control logic developed within the LabVIEW environment [47]. In particular, the following parameters can be set by users: (i) indoor air temperature ($T_{SP,Room}$) and relative humidity ($RH_{SP,Room}$) targets to be achieved in the test room; (ii) deadbands (DB_T and DB_{RH}) associated with indoor air temperature and humidity targets; (iii) percentage velocity of the return air fan (OL_{RAF}) and the supply air fan (OL_{SAF}) within the range between 0% and 100%; (iv) opening percentages of the return air damper (OP_{DRA}), the outside air damper (OP_{DOA}), the exhaust air damper (OP_{DEA}), and the heat recovery system damper (OP_{DHRS}) within the range 0%÷100%. Activation/deactivation of the HVAC components (HUM valve, CC valve, PostHC valve, HP, PHP, RS, and PRS) is based on predefined conditions listed in Table 3, regardless of the season (the control logic of the PreHC is not included in this table as it was intentionally set to off-mode throughout all the tests conducted in this study). Particularly, the HP is activated only when the temperature of the heat carrier fluid (T_{HT}) inside the hot tank (HT) is less than the selected set-point temperature ($T_{HT,SP}$) by a defined deadband temperature ($DB_{T,HT}$);

Table 3
Conditions for activating/deactivating the main AHU components.

	ON	OFF
Humidifier valve	$RH_{RA} \leq (RH_{SP,Room} - DB_{RH})$	$RH_{RA} \geq (RH_{SP,Room} + DB_{RH})$
Cooling coil valve	$T_{RA} \geq (T_{SP,Room} + DB_T)$ OR $RH_{RA} \geq (RH_{SP,Room} + DB_{RH})$	$T_{RA} \leq (T_{SP,Room} - DB_T)$ AND $RH_{RA} \leq (RH_{SP,Room} - DB_{RH})$
Post-heating coil valve	$T_{RA} \leq (T_{SP,Room} - DB_T)$	$T_{RA} \geq (T_{SP,Room} + DB_T)$
Heat Pump	$T_{HT} < (T_{HT,SP} - DB_{T,HT})$	$T_{HT} \geq (T_{HT,SP} + DB_{T,HT})$
Circulating pump of the heat pump	$T_{RA} \leq (T_{SP,Room} - DB_T)$	$T_{RA} \geq (T_{SP,Room} + DB_T)$
Refrigerating system	$T_{CT} > (T_{CT,SP} + DB_{T,CT})$	$T_{CT} \leq (T_{CT,SP} - DB_{T,CT})$
Circulating pump of the refrigerating system	$T_{RA} \geq (T_{SP,Room} + DB_T)$ OR $RH_{RA} \geq (RH_{SP,Room} + DB_{RH})$	$T_{RA} \leq (T_{SP,Room} - DB_T)$ AND $RH_{RA} \leq (RH_{SP,Room} - DB_{RH})$

then it keeps running till temperature of the heat carrier fluid is equal to ($T_{HT,SP} + DB_{T,HT}$). With respect to the RS, it is activated only if temperature of the heat carrier fluid (T_{CT}) inside the cold tank (CT) is greater than the defined set-point temperature ($T_{CT,SP}$) by the defined deadband temperature ($DB_{T,CT}$); then, it keeps running until the heat carrier fluid temperature is equal to ($T_{CT,SP} - DB_{T,CT}$).

PID (Proportional-Integral-Derivative) controllers automatically adjust the opening percentages of the valves supplying (i) the post-heating coil (OP_{V_PostHC}), (ii) the cooling coil (OP_{V_CC}), and (iii) the humidifier (OP_{V_HUM}) to maintain the return air temperature and relative humidity within specified deadbands. The specified upper and lower deadbands of T_{RA} are, respectively, UDB_T ($UDB_T = T_{SP,Room} + DB_T$) and LDB_T ($LDB_T = T_{SP,Room} - DB_T$), while the upper and lower deadbands of RH_{RA} are, respectively, UDB_{RH} ($UDB_{RH} = RH_{SP,Room} + DB_{RH}$) and the lower bound LDB_{RH} ($LDB_{RH} = RH_{SP,Room} - DB_{RH}$).

For the PostHC, the PID controller parameters P and I are set to 1000, while D is set to 10; in the case of the CC, the PID controller parameter P is set to –1000, while I and D are set to 1000 and 10, respectively. Finally, for the HUM, the PID controller parameters P, I and D, respectively, are set to 1000, 10,000 and 500.

End-users have the option to manually override the operation of specific components and simulate the occurrence of specific faults' types/severities for defined research purposes. In particular, they can force (i) the opening percentages of valves, (ii) the return air temperature and relative humidity sensors' readings, (iii) the percentage velocity of the supply air fan and the return air fan.

3. Methodology and design of experiments

The performance of the AHU serving the integrated test room in the SENS i-Lab has been examined through a total of 36 experimental tests conducted under varying summer and winter conditions. Notably, 14 experiments have been conducted under normal (N) conditions to assess normal operation; in more detail, 6 tests (SN1, SN2, SN3, SN4, SN5 and SN6) have been performed during the summer (S), while the other 8 tests (WN1, WN2, WN3, WN4, WN5, WN6, WN7, and WN8) have been performed during the winter (W). The remaining 22 faulty (F) tests (SF1, SF2, SF3, SF4, SF5, SF6, SF7, SF8, SF9, SF10, SF11, WF1, WF2, WF3, WF4, WF5, WF6, WF7, WF8, WF9, WF10 and WF11) have been performed during both summer (S) and winter (W) with 11 faulty tests per season; in each faulty test, a particular fault type/severity has been analysed by manually forcing the operation of specific components in order to artificially simulate the occurrence of faulty conditions. A single fault severity has been considered for some of the above-mentioned faults types, while two severity levels have been considered for the remaining faults types investigated in this study. In addition, each fault type/severity has been studied individually.

During the normal tests the following parameters are manually set: (i) the indoor air temperature setpoint ($T_{SP,Room}$) is 20 °C in winter and 26 °C in summer, with a deadband (DB_T) of ± 1 °C; (ii) the indoor air relative humidity setpoint ($RH_{SP,Room}$) is 50% during both seasons, with a deadband (DB_{RH}) of ± 5%; (iii) the supply and return air fans are set to operate with a percentage velocity (OL_{SAF}, OL_{RAF}) at 50% of their maximum velocities; (iv) the opening percentages of the return air damper (OP_{DRA}), the outdoor air damper (OP_{DOA}) and the exhaust air damper (OP_{DEA}) are equal to 100%, 20% and 20%, respectively. The heat recovery system is not activated ($OP_{DHRS} = 100\%$), while the cooling coil valve, the humidifier valve and the post-heating coil valve opening percentages can vary between 0 ÷ 100% according to the AHU control logic in order to keep the desired indoor conditions. The faulty tests have been conducted using the same settings as the normal ones, except the operation of the return and supply air fans, the cooling coil valve, the humidifier valve, the post-heating coil valve, and the return air temperature/relative humidity sensor.

Table 4 outlines the boundary conditions corresponding to the faulty experiments with the cells in yellow highlighting the faulty component as well as the corresponding fault severity.

As shown in Table 4, 11 fault types/severities have been experimentally examined by intentionally introducing the fault at the start of the tests (always set at 9:00 a.m.) and maintaining it until the end of the experiments (always concluding at 6:00 p.m.). Specifically, the following 11 fault types/severities have been considered:

- fault 1: positive offset of +15% was artificially applied and kept to the readings of the return air relative humidity sensor through the faulty tests SF1 and WF1;
- fault 2: negative offset equal to –15% was artificially applied and kept constant to the readings of the return air relative humidity sensor through the faulty tests SF2 and WF2;
- fault 3: a negative offset equal to –3.0 °C was artificially applied from the return air temperature sensor readings through the faulty tests SF3 and WF3;
- fault 4: over the faulty tests SF4 and WF4, the humidifier valve remained consistently closed (stuck at 0%);
- fault 5: a positive offset equal to +3.0 °C was purposely applied to the return air temperature sensor readings during the faulty tests SF5 and WF5;
- fault 6: the cooling coil valve remained fully open (stuck at 100%) throughout the faulty tests SF6 and WF6;
- fault 7: the post-heating coil valve remained closed (stuck at 0%) throughout the faulty tests SF7 and WF7;
- fault 8: the post-heating coil valve remained fully open (stuck at 100%) throughout the faulty tests SF8 and WF8;
- fault 9: the cooling coil valve remained fully closed (stuck at 0%) throughout the faulty tests SF9 and WF9;
- fault 10: complete failure of the return air fan (instead of a nominal velocity of 50%), implemented during the faulty tests SF10 and WF10;
- fault 11: corresponding to a complete failure of the supply air fan (instead of a nominal velocity of 50%) implemented during the faulty tests SF11 and WF11.

The investigation did not include the scenario where the humidifier is stuck at 100% due to potential technical complications. This situation could trigger condensation phenomena, posing risks to the integrity of the laboratory's devices and sensors. Additionally, the pre-heating coil has been manually deactivated and not used during any experiments. For all tests, both normal and faulty, all parameters listed in Table 2 were measured at 1-second intervals.

Table 4
Boundary conditions of the faulty experiments.

ID	Date (d/m/y)	$T_{SP,Room}$ (°C)	Offset of T_{RA} sensor (°C)	Offset of RH_{RA} sensor (%)	OL_{SAF} (%)	OL_{RAF} (%)	OP_{V_PostHC} (%)	OP_{V_CC} (%)	OP_{V_HUM} (%)
SF1	22/07/2021	26	0	15	50	50	0÷100	0÷100	0÷100
SF2	26/07/2021		0	−15	50	50	0÷100	0÷100	0÷100
SF3	02/08/2021		−3	0	50	50	0÷100	0÷100	0÷100
SF4	04/08/2021		0	0	50	50	0÷100	0÷100	0
SF5	05/08/2021		3	0	50	50	0÷100	0÷100	0÷100
SF6	25/08/2021		0	0	50	50	0÷100	100	0÷100
SF7	26/08/2021		0	0	50	50	0	0÷100	0÷100
SF8	30/08/2021		0	0	50	50	100	0÷100	0÷100
SF9	01/09/2021		0	0	50	50	0÷100	0	0÷100
SF10	07/09/2021		0	0	50	0	0÷100	0÷100	0÷100
SF11	08/09/2021		0	0	0	50	0÷100	0÷100	0÷100
WF1	16/02/2022		0	15	50	50	0÷100	0÷100	0÷100
WF2	29/12/2021		0	−15	50	50	0÷100	0÷100	0÷100
WF3	21/12/2021		−3	0	50	50	0÷100	0÷100	0÷100
WF4	09/02/2022	20	0	0	50	50	0÷100	0÷100	0
WF5	02/02/2022		3	0	50	50	0÷100	0÷100	0÷100
WF6	07/03/2022		0	0	50	50	0÷100	100	0÷100
WF7	16/12/2021		0	0	50	50	0	0÷100	0÷100
WF8	13/12/2021		0	0	50	50	100	0÷100	0÷100
WF9	31/01/2022		0	0	50	50	0÷100	0	0÷100
WF10	20/12/2021		0	0	50	0	0÷100	0÷100	0÷100
WF11	17/12/2021		0	0	0	50	0÷100	0÷100	0÷100

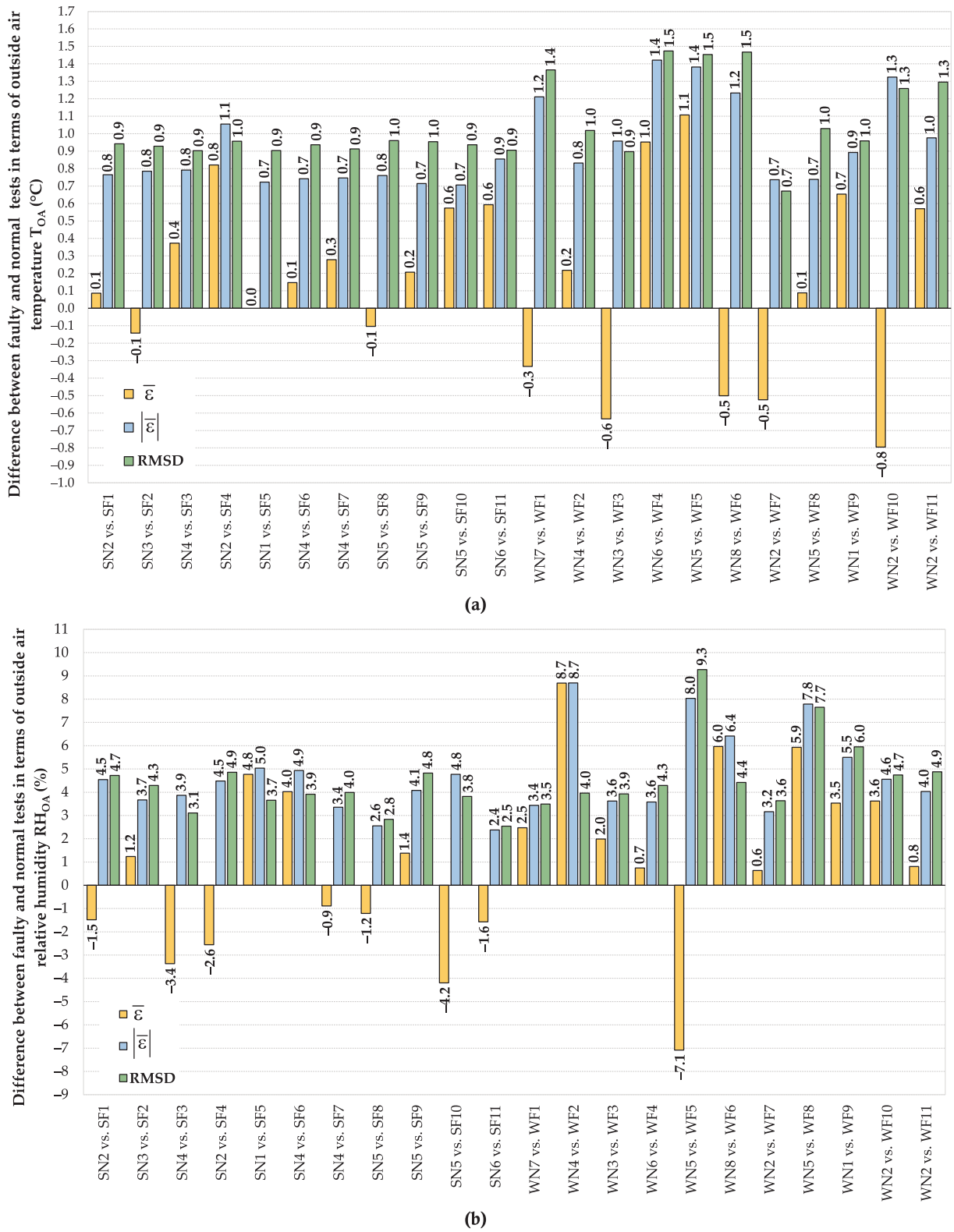


Fig. 2. Comparison of normal and faulty tests in terms of outside air temperature T_{OA} (a) and outside air relative humidity RH_{OA} (b).

4. Assessment of boundary conditions between normal and faulty tests

The normal tests (SN1–SN6 and WN1–WN8) have been considered as reference baselines for comparison with the faulty tests (SF1–SF11 and WF1–WF11) to evaluate the effects related with the occurrence of the chosen fault types/severities. It's worth noting that all the experiments (faulty and normal) conducted during summer started with the same initial indoor air temperature (approximately 28 °C) and relative humidity (around 60%). Similarly, tests (faulty and normal) performed during winter began with a similar initial indoor air temperature (around 18 °C) and relative humidity (approximately 60%). Further

details regarding the comparison of boundary conditions between normal and faulty tests can be found in [40,41]. The comparability of the normal tests in contrast to the faulty ones has been initially proved by comparing the boundary conditions of the experiments in terms of outside air temperature (T_{OA}) and relative humidity (RH_{OA}) by using the following metrics:

$$\varepsilon_i = EXP_{OA,Faulty,i} - EXP_{OA,Baseline,i} \tag{16}$$

$$\overline{\varepsilon} = \sum_{i=1}^{N} \frac{\varepsilon_i}{N} \tag{17}$$

$$|\overline{\varepsilon}| = \sum_{i=1}^{N} \frac{|\varepsilon_i|}{N} \tag{18}$$

$$RMSD = \sqrt{\sum_{i=1}^{N} \frac{(\varepsilon_i - \overline{\varepsilon})^2}{N}} \tag{19}$$

where $EXP_{OA,Faulty,i}$ and $EXP_{OA,Baseline,i}$ are, respectively, the experimental values of RH_{OA}/T_{OA} at the i-th time step under faulty and normal conditions, $\overline{\varepsilon}$ is the average difference between baseline and faulty tests, $|\overline{\varepsilon}|$ is the average absolute difference between baseline and faulty tests, RMSD is the root mean square difference between baseline and faulty tests, N is the number of experimental data points. A normal test has been considered comparable with faulty test only in case of all the above-mentioned three statistical metrics are lower than 1.5 °C for T_{OA} and 10% for RH_{OA}.

Fig. 2 reports the values of $\overline{\varepsilon}$, $|\overline{\varepsilon}|$ and RMSD derived by comparing the most similar normal and faulty tests among the above-mentioned experiments based on of T_{OA} and RH_{OA}.

Fig. 2 illustrates the maximum values of $\overline{\varepsilon}$, $|\overline{\varepsilon}|$ and RMSD reaching up to 1.1 °C, 1.4 °C, and 1.5 °C for T_{OA}, respectively, and 8.7%, 8.7%, and 9.3% for RH_{OA}. According to the methodology outlined by Granderson et al. [20], the boundary conditions of the compared normal and faulty tests can be considered highly close according to the data depicted in Fig. 2. Specifically:

- the normal test SN1 is comparable with the faulty test SF5;
- the normal test SN2 is comparable with the faulty tests SF1 and SF4;
- the normal test SN3 is comparable with the faulty test SF2;
- the normal test SN4 is comparable with the faulty tests SF3, SF6 and SF7;
- the normal test SN5 is comparable with the faulty tests SF8, SF9 and SF10;
- the normal test SN6 is comparable to the faulty test SF11;
- the normal test WN1 is comparable with the faulty test WF9;
- the normal test WN2 is comparable with the faulty tests WF7, WF10 and WF11;
- the normal test WN3 is comparable with the faulty test WF3;
- the normal test WN4 is comparable with the faulty test WF2;
- the normal test WN5 is comparable with the faulty tests WF5 and WF8;
- the normal test WN6 is comparable with the faulty test WF4;
- the normal test WN7 is comparable to the faulty test WF1;
- the normal test WN8 is comparable with the faulty test WF6.

Therefore, comparing the aforementioned faulty and normal tests enables for evaluating the impacts related to the occurrence of the selected faults on the AHU operation.

5. Results and discussion

In this section all the results obtained during the experimental campaign are presented. It should be underlined that some aspects make the study's content and, therefore, its results unique. In addition to the different AHU scale, this is mainly related to the inclusion of the humidification subsystem, which is almost entirely absent from comparable fault datasets; furthermore, a specifically-developed control logic has been developed in order to manage the AHU components and guarantee the desired indoor conditions; moreover, data were collected at high temporal resolution (1-second sampling), allowing for the capture of short-duration dynamics and transient effects that are often lost in other studies; finally, this work spans Mediterranean conditions under multiple seasons, which have only been minimally investigated in other studies.

In particular, the next subsections describe the faults' impacts in terms of indoor thermo-hygrometric conditions (5.1), electrical power (5.2) electric energy demand (5.3), operational costs (5.4), global equivalent CO_2 emissions (5.5) as well as operating times of AHU components (5.6). Section 5.7 provides an integrated discussion of the faults' impacts across all the above-mentioned parameters. Finally, Section 5.8 performs a comparative analysis of faults based on these impacts.

5.1. Indoor thermo-hygrometric conditions

In this section the impacts of the investigated faults on indoor air temperature and relative humidity are analysed. In greater detail, the percentages of time during which indoor air temperature (TMR) or indoor air relative humidity (RHMR) is maintained within the specified deadbands for each normal and corresponding faulty test are calculated via the following formulas based on the measured data:

$$TMR = \frac{N_{in,DBT}}{N} \cdot 100 \tag{20}$$

$$RHMR = \frac{N_{in,DBRH}}{N} \cdot 100 \tag{21}$$

where:

- $N_{in,DBT}$ represents the number of experimental data points throughout the test duration when T_{RA} falls within its corresponding deadbands;
- $N_{in,DBRH}$ represents the number of experimental data points throughout the test duration when RH_{RA} falls within its corresponding deadbands;
- N denotes the total number of recorded data points per test (considering a 1-second sampling rate and a daily operating period from 9:00 a.m. to 6:00 p.m., this leads to have 32,400 experimental data points).

Additionally, the relevance of deviations from desired indoor air temperatures $|\overline{\varepsilon}_{T,D}|$ and the relevance of deviations from desired indoor air relative humidity $|\overline{\varepsilon}_{RH,D}|$ are defined based on the experimental data as follows:

$$|\overline{\varepsilon}_{T,D}| = \frac{1}{N_{out,DBT}} \cdot \left(\sum_{i=1}^{N} |\Delta T_{out,DBT,i}| \quad | \quad T_{RA,i} \notin [LDB_T, UDB_T] \right) \tag{22}$$

$$|\overline{\varepsilon}_{RH,D}| = \frac{1}{N_{out,DBRH}} \cdot \left(\sum_{i=1}^{N} |\Delta RH_{out,DBRH,i}| \quad | \quad RH_{RA,i} \notin [LDB_{RH}, UDB_{RH}] \right) \tag{23}$$

where:

- $\Delta T_{out,DBT}$ is the deviation of actual return air temperature from the desired temperature boundaries; it's only computed when actual T_{RA} falls outside the upper deadband (UDB_T) or the lower deadband (LDB_T) of $RH_{SP,Room}$;

Table 5
Daily indoor air temperature/relative humidity met ratios together with relevance of deviations from desired indoor air temperature/relative humidity.

Test ID	TMR (%)	RHMR (%)	$\lvert\bar{\varepsilon}_{T,D}\rvert$ (°C)	$\lvert\bar{\varepsilon}_{RH,D}\rvert$ (%)
SF1	76.0	25.4	0.1	2.2
SN2	71.6	92.2	0.4	1.8
SF2	88.1	0.6	0.4	11.9
SN3	76.0	89.9	0.4	2.5
SF3	0.0	75.4	2.1	1.8
SN4	74.8	91.8	0.3	2.0
SF4	67.8	96.1	0.2	1.1
SN2	71.6	92.2	0.4	1.8
SF5	2.5	59.4	1.9	2.4
SN1	68.8	83.5	0.3	3.4
SF6	73.7	94.1	0.2	0.7
SN4	74.8	91.8	0.3	2.0
SF7	2.6	57.8	3.8	2.5
SN4	74.8	91.8	0.3	2.0
SF8	0.0	90.1	2.5	0.9
SN5	69.4	86.2	0.3	3.1
SF9	1.9	76.2	2.0	5.4
SN5	69.4	86.2	0.3	3.1
SF10	70.5	86.0	0.3	3.4
SN5	69.4	86.2	0.3	3.1
SF11	58.7	31.3	0.2	1.2

(*continued on next page*)

Table 5 (*continued*)

Test ID	TMR (%)	RHMR (%)	$\lvert\bar{\varepsilon}_{T,D}\rvert$ (°C)	$\lvert\bar{\varepsilon}_{RH,D}\rvert$ (%)
SN6	77.3	93.3	0.2	3.8
WF1	76.4	96.3	0.3	1.8
WN7	76.3	95.3	0.3	1.5
WF2	72.0	0.0	0.5	8.7
WN4	78.0	90.9	0.2	1.4
WF3	8.2	86.8	1.9	1.2
WN3	75.2	95.3	0.2	1.5
WF4	80.5	18.4	0.3	2.6
WN6	77.2	90.9	0.5	0.9
WF5	0.0	95.8	1.6	0.7
WN5	78.2	92.5	0.5	0.6
WF6	74.0	87.7	0.3	1.3
WN8	73.7	90.8	0.3	1.3
WF7	0.0	0.0	3.0	2.9
WN2	75.8	96.8	0.2	1.2
WF8	5.5	88.5	3.9	0.7
WN5	78.2	92.5	0.5	0.6
WF9	18.5	97.7	0.6	2.5
WN1	76.9	97.1	0.2	2.0
WF10	76.3	89.6	0.3	2.5
WN2	75.8	96.8	0.2	1.2
WF11	74.8	98.1	0.2	1.2
WN2	75.8	96.8	0.2	1.2

- $\Delta RH_{out,DBRH}$ is the deviation from the desired relative humidity range of actual return air relative humidity; it's only computed when actual RH_{RA} falls outside the upper deadband (UDB_{RH}) or the lower deadband (LDB_{RH}) of $RH_{SP,Room}$;
- $N_{out,DBT}$ represents the total number of data points during which return air temperature is outside the acceptable range;
- $N_{out,DBRH}$ represents the total number of data points during which return air relative humidity is outside the acceptable range.

Table 5 reports the values of parameters calculated via Eqs. (20–23), with the worst values highlighted by red font and the best values indicated by green font only in case of faulty tests. Table 5 indicates that daily indoor air temperature/relative humidity met ratios are below 100% during normal tests; this is due to the AHU's transient operation, especially during the start-up of the system at the beginning of the tests. The minimum values of TMR, RHMR, $|\overline{\varepsilon}_{T,D}|$ and $|\overline{\varepsilon}_{RH,D}|$ are 0.0%, 0.0%, 0.1 °C and 0.7%, respectively, while the maximum values of TMR, RHMR, $|\overline{\varepsilon}_{T,D}|$ and $|\overline{\varepsilon}_{RH,D}|$ are 88.1%, 98.1%, 3.9 °C and 11.9%, respectively. In some cases, the values of TMR or RHMR in the case of normal tests are slightly lower (from a minimum of approximately 1% to a maximum of about 4%) than those for the corresponding faulty tests; these differences are attributable to the minimal differences in terms of outside as well as initial indoor air conditions. With reference to the comparison between the normal test SN3 and the faulty test SF2, the difference in terms of TMR, in addition to being linked to the minimal differences in terms of outside as well as initial indoor air conditions, is mainly attributable to the fact that the cooling coil in the case of the faulty test is much less used than in the case of the normal test (due to lower dehumidification requirements caused by the incorrect reading of indoor air relative humidity due to the occurrence of the fault), so the cooling process during the faulty test is slower due to the thermal inertia of the cooling coil itself with respect to the normal test.

In addition to the above-mentioned metrics, Lu et al. [32] suggested the following key performance indexes (KPIs): (i) the absolute maximum indoor air temperature deviation (dT_{max}) calculated as the largest absolute deviation between actual return air temperature T_{RA} and the upper or lower $T_{SP,Room}$ deadband; (ii) the absolute total indoor air temperature deviation (dT_{tot}) defined by adding all indoor air temperature absolute deviations over the entire test period; (iii) the absolute maximum indoor air relative humidity deviation (dRH_{max}) calculated as the largest absolute deviation between actual return air relative humidity RH_{RA} and the upper or lower $RH_{SP,Room}$ deadband; (iv) the absolute total indoor air relative humidity deviation (dRH_{tot}) defined by adding all indoor air relative humidity absolute deviations, over the entire duration of the test. The above-mentioned KPIs have been calculated for both normal and faulty tests according to the following equations:

$$dT_{\max} = \max\left|\Delta T_{out,DBRH,i}\right| \quad | \quad T_{RA,i} \notin [LDB_T, UDB_T] \tag{24}$$

$$dT_{tot} = \sum_{i=1}^{N} \left|\Delta T_{out,DBT,i}\right| \quad | \quad T_{RA,i} \notin [LDB_T, UDB_T] \tag{25}$$

$$dRH_{\max} = \max\left|\Delta RH_{out,DBRH,i}\right| \quad | \quad RH_{RA,i} \notin [LDB_{RH}, UDB_{RH}] \tag{26}$$

$$dRH_{tot} = \sum_{i=1}^{N} \left|\Delta RH_{out,DBRH,i}\right| \quad | \quad RH_{RA,i} \notin [LDB_{RH}, UDB_{RH}] \tag{27}$$

The percentage difference of the previous parameters between faulty and normal tests has been also calculated as follows:

$$\%d = \frac{\left(d_{\text{Faulty}} - d_{\text{Baseline}}\right)}{d_{\text{Baseline}}} \cdot 100 \tag{28}$$

where:

- d_{Faulty} are the values of dT_{max}, dT_{tot}, dRH_{max}, and dRH_{tot} associated to the corresponding faulty experiments;
- $d_{Baseline}$ represents the values of dT_{max}, dT_{tot}, dRH_{max}, and dRH_{tot} corresponding to the normal tests.

A positive %d indicates that the value of the corresponding metric during the normal test is lower than that one observed in the related faulty test, which means that during the faulty experiment the AHU is able to control in a worse way the associated indoor parameter in comparison to the normal experiment. Table 6 reports the values of %d (calculated via Eq. (28) of the KPIs defined by Eqs. (24–27) for each pair of tests under comparison during summer and winter, while the absolute values of the above-mentioned KPIs associated for each normal/faulty test are reported in Table A.1 in the Appendix A. The cells displaying the values of %d in Table 6 are color-coded according to the legend reported at the end of this table (cells are in yellow if %d is included in the range ± 10%, in red if %d is greater than 20% or lower than –20%, in orange in all other cases). The minimum values of dT_{max}, dT_{tot}, dRH_{max} and dRH_{tot} are –20.7%, –69.2%, –43.7% and –79.9%, respectively, while the maximum positive values of dT_{max}, dT_{tot}, dRH_{max} and dRH_{tot} are 409.3%, 7270.1%, 284.0% and 7347.4%, respectively. The negative values in Table 6 are due, as already explained with reference to Table 5, to the minimal differences in terms of outdoor air conditions as well as initial indoor air conditions between the corresponding normal and faulty tests. In some cases the percentage differences in Table 6 are very significant as the values of the relative metric are very small in the case of the corresponding normal or faulty tests.

5.2. Effects of faults on electrical power demand of AHU components

In this section the effects of the tested faults in terms of power demand are presented. The measurement uncertainty associated to power consumption of AHU components has been assessed by using Eqs. 8–14. Based on field data, the largest average absolute errors for $P_{el,SAF}$, $P_{el,RAF}$, $P_{el,RS}$, $P_{el,PRS}$, $P_{el,HP}$, $P_{el,PHP}$ and $P_{el,HUM}$ are 24.3 W, 2.8 W, 100.3 W, 96.9 W, 101.7 W, 98.4 W and 26.1 W, respectively. These absolute errors correspond to maximum average relative uncertainties of 7.0%, 3.7%, 4.7%, 12.2%, 5.7%, 12.3% and 2.1%, respectively.

For each normal/faulty experiment as well as AHU components, Table 7 reports the parameters $\%\mu_{el}$ and $\%\sigma_{el}$ defined as follows upon varying both the pair of tests under comparison as well as the AHU component:

$$\%\mu_{el} = \frac{\left(\mu_{el,\text{Faulty}} - \mu_{el,\text{Baseline}}\right)}{\mu_{el,\text{Baseline}}} \cdot 100 \tag{29}$$

$$\%\sigma_{el} = \frac{\left(\sigma_{el,\text{Faulty}} - \sigma_{el,\text{Baseline}}\right)}{\sigma_{el,\text{Baseline}}} \cdot 100 \tag{30}$$

where $\mu_{el,Faulty}$ and $\mu_{el,Baseline}$ are, respectively, the arithmetic mean μ_{el} of electric power consumption P_{el} during faulty and baseline tests, while $\sigma_{el,Faulty}$ and $\sigma_{el,Baseline}$ are, respectively, the standard deviation σ_{el} of electric power consumption P_{el} during faulty and baseline tests. The values of the $\mu_{el,Baseline}$, $\mu_{el,Faulty}$, $\sigma_{el,Baseline}$ and $\sigma_{el,Faulty}$ are reported in Table A.2 in Appendix A. In Table 7 the cells reporting the values of $\%\mu_{el}$ and $\%\sigma_{el}$ are filled in yellow if $\%\mu_{el}$ or $\%\sigma_{el}$ is included in the range ± 10%, in red if $\%\mu_{el}$ or $\%\sigma_{el}$ is greater than 20% or lower than –20%, in orange in other cases (the symbol N.A. (not applicable) denotes that the AHU component has not been activated during both tests and the calculation of $\%\mu_{el}$ or $\%\sigma_{el}$ cannot be performed, while the symbol '∞' indicates that the AHU component has not been activated only during the normal test). In Table 7 the circulating pumps PRS and PHP are not reported because for those auxiliary systems a faulty condition can only affect their operation times, but does not significantly influence their power consumption while operating.

According to Lu et al. [32], the percentage difference $\%P_{el,max}$

Table 6
Values of %d (calculated via Eq. (28) for dT_{max}, dT_{tot}, dRH_{max}, and dRH_{tot} for the corresponding faulty and normal tests during summer and winter.

	dT_{max}	dT_{tot}	dRH_{max}	dRH_{tot}
$\%d_{SF1\ vs.\ SN2}$ (%)	–10.3	–69.2	–23.1	1068.5
$\%d_{SF2\ vs.\ SN3}$ (%)	6.3	–52.1	200.0	4547.1
$\%d_{SF3\ vs.\ SN4}$ (%)	203.7	2686.5	–14.0	175.0
$\%d_{SF4\ vs.\ SN2}$ (%)	–1.6	–30.3	–12.5	–69.0
$\%d_{SF5\ vs.\ SN1}$ (%)	168.8	1844.4	–43.7	73.9
$\%d_{SF6\ vs.\ SN4}$ (%)	33.6	–22.2	–38.2	–74.3
$\%d_{SF7\ vs.\ SN4}$ (%)	409.3	4779.3	–1.0	554.2
$\%d_{SF8\ vs.\ SN5}$ (%)	148.9	2402.7	–34.4	–79.9
$\%d_{SF9\ vs.\ SN5}$ (%)	169.2	1896.7	20.9	203.9
$\%d_{SF10\ vs.\ SN5}$ (%)	–12.8	–14.0	55.4	10.4
$\%d_{SF11\ vs.\ SN6}$ (%)	–20.7	160.5	–27.6	229.2
$\%d_{WF1\ vs.\ WN7}$ (%)	4.2	0.7	4.6	–3.8
$\%d_{WF2\ vs.\ WN4}$ (%)	4.0	216.4	284.0	6604.7
$\%d_{WF3\ vs.\ WN3}$ (%)	252.6	3936.9	–13.1	129.1
$\%d_{WF4\ vs.\ WN6}$ (%)	–9.4	–48.5	54.8	2503.0
$\%d_{WF5\ vs.\ WN5}$ (%)	74.8	1327.6	39.4	–38.2
$\%d_{WF6\ vs.\ WN8}$ (%)	4.9	14.8	63.3	37.2
$\%d_{WF7\ vs.\ WN2}$ (%)	376.7	7270.1	22.1	7347.4
$\%d_{WF8\ vs.\ WN5}$ (%)	360.6	3078.7	49.6	62.5
$\%d_{WF9\ vs.\ WN1}$ (%)	–3.6	1064.6	21.6	–2.2
$\%d_{WF10\ vs.\ WN2}$ (%)	2.2	58.0	159.8	583.1
$\%d_{WF11\ vs.\ WN2}$ (%)	11.1	–7.3	–29.6	–42.1

Legend

	$-10\% \leq \%d \leq +10\%$
	$+10\% < \%d \leq +20\%$ OR $-20\% \leq \%d < -10\%$
	$\%d > +20\%$ OR $\%d < -20\%$

Table 7
Values of $\%\mu_{el}$ (calculated via Eq. (29) and $\%\sigma_{el}$ (calculated via Eq. (30) upon varying both the pair of tests under comparison as well as the AHU component.

	$\%\mu_{el}$ (%)	$\%\sigma_{el}$ (%)	$\%\mu_{el}$ (%)	$\%\sigma_{el}$ (%)	$\%\mu_{el}$ (%)	$\%\sigma_{el}$ (%)	$\%\mu_{el}$ (%)	$\%\sigma_{el}$ (%)	$\%\mu_{el}$ (%)	$\%\sigma_{el}$ (%)
SF1 vs. SN2	–0.4	–3.7	–0.1	–4.0	–1.1	–0.4	–0.4	–0.6	–100.0	–100.0
SF2 vs. SN3	–1.4	32.7	–0.2	36.8	14.7	–69.4	22.9	–69.3	9.8	–48.3
SF3 vs. SN4	–1.3	1.4	0.0	10.9	–0.3	–1.4	–0.7	–4.4	0.1	–1.9
SF4 vs. SN2	2.1	68.8	–0.4	96.4	28.6	–38.8	48.5	–69.7	–100.0	–100.0
SF5 vs. SN1	0.8	65.3	–1.2	–14.8	41.3	–69.9	52.4	–67.2	–100.0	–100.0
SF6 vs. SN4	1.1	1.1	0.5	–3.8	–0.3	–28.3	–1.0	5.9	1.5	–6.5
SF7 vs. SN4	3.3	–0.1	0.8	–3.1	–0.1	–19.8	–100.0	–100.0	–100.0	–100.0
SF8 vs. SN5	–1.0	–9.5	–0.8	–0.5	1.2	–43.1	0.0	–2.6	5.6	–31.6
SF9 vs. SN5	–1.1	–6.4	–0.9	2.9	2.8	–26.0	–100.0	–100.0	–5.2	38.6
SF10 vs. SN5	–3.3	11.3	–77.1	–98.3	1.3	–33.7	–0.9	3.2	1.0	–4.0
SF11 vs. SN6	–72.5	–67.2	–3.6	22.4	0.9	8.4	4.0	–16.4	N.A.	N.A.
WF1 vs. WN7	0.0	–3.9	–0.2	–0.9	0.3	0.5	0.9	–8.9	N.A.	N.A.
WF2 vs. WN4	–0.2	1.1	–1.2	3.7	–1.0	6.8	0.2	–12.8	∞	∞
WF3 vs. WN3	–1.0	–5.6	0.0	–41.8	0.3	–8.8	0.2	–5.0	6.2	–21.2
WF4 vs. WN6	–0.1	–0.3	0.3	–18.5	0.2	0.1	–0.1	–1.8	–100.0	–100.0
WF5 vs. WN5	0.8	–32.1	0.2	–68.8	0.7	–7.9	0.6	–3.3	–5.4	21.7
WF6 vs. WN8	–0.4	–1.4	0.1	–5.1	12.8	11.4	–0.3	36.9	0.9	–3.8
WF7 vs. WN2	2.4	–16.4	0.8	–16.3	–0.6	–7.4	1.8	–22.8	–100.0	–100.0
WF8 vs. WN5	–4.4	–10.6	–0.7	–56.0	0.1	–4.3	–6.1	16.7	4.4	–19.1
WF9 vs. WN1	1.7	–73.1	–2.4	–1.9	0.5	–5.7	–0.2	4.9	N.A.	N.A.
WF10 vs. WN2	–2.3	3.0	–77.6	–97.9	–0.1	–10.1	0.0	6.0	12.4	–35.5
WF11 vs. WN2	–74.8	–90.0	–2.9	8.9	0.9	–1.1	1.5	–21.4	–100.0	–100.0

Legend

	$-10\% \leq \%\mu_{el}, \%\sigma_{el} \leq +10\%$
	$+10\% < \%\mu_{el}, \%\sigma_{el} \leq +20\%$ OR $-20\% \leq \%\mu_{el}, \%\sigma_{el} < -10\%$
	$\%\mu_{el}, \%\sigma_{el} > +20\%$ OR $\%\mu_{el}, \%\sigma_{el} < -20\%$

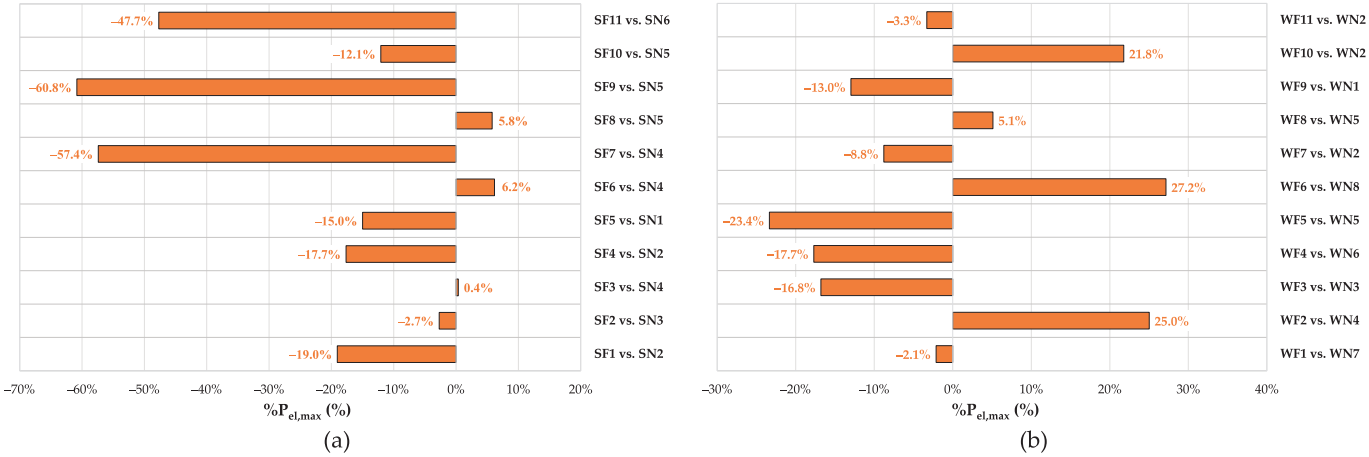


Fig. 3. Percentage difference between normal and faulty tests in terms of maximum electrical power demand during summer (a) and winter (b).

between faulty and normal tests in terms of maximum electrical power demand of AHU components has been calculated for both normal and faulty tests via the following equation:

$$\%P_{el,max} = \frac{(P_{el,max,Faulty} - P_{el,max,Baseline})}{P_{el,max,Baseline}} \cdot 100 \quad (31)$$

where $P_{el,max,Faulty}$ and $P_{el,max,Baseline}$ are, respectively, the peak electric power demand during the faulty experiment and the corresponding normal test, respectively. Fig. 3 reports the value of $\%P_{el,max}$ as a function of the pairs of tests under comparison.

Fig. 3 indicates that the values of $\%P_{el,max}$ are generally relevant and vary from a minimum of –61% (corresponding to the comparison between the faulty test SF9 and the normal test SN5) up to a maximum of 27% (corresponding to the comparison between the faulty test WF6 and the normal test WN8).

5.3. Effects of faults on daily electrical energy consumption

In this section the effects of the selected faults in terms of daily electric energy consumption are analysed. Table 8 reports the percentage difference $\%E_{el}$ between faulty and corresponding normal experiments in terms of daily electric energy consumption referred to the operation of (1) the supply air fan, (2) the return air fan, (3) the refrigerating system and its circulating pump, (4) the heat pump and its circulating pump, (5) the steam humidifier, as well as (6) the entire AHU during summer and winter. This percentage difference $\%E_{el}$ is calculated as follows:

$$\%E_{el} = \frac{(E_{el,Faulty} - E_{el,Baseline})}{E_{el,Baseline}} \cdot 100 \quad (32)$$

where $E_{el,Faulty}$ and $E_{el,Baseline}$ are, respectively, the daily electric energy consumption during faulty and corresponding normal experiment. The values of $E_{el,Baseline}$ and $E_{el,Faulty}$ are reported in Table A.3 in Appendix A upon varying both normal/faulty test and AHU component. The cells in Table 8 are filled in yellow if $\%E_{el}$ is included in the range ± 10%, in red if $\%E_{el}$ is greater than 20% or lower than –20%, in orange in other cases (the symbol N.A. denotes that the AHU component has not been activated during both tests and the calculation of $\%E_{el}$ is not applicable, while the symbol '∞' indicates that the AHU component has not been activated only during the normal test). According to Table 8, the values of $\%E_{el}$ corresponding to the total daily electric demand range from –80.5% up to 82.9%.

5.4. Effects of faults on operational costs

In this section the effects of the selected faults in terms of daily operating costs are discussed. The percentage difference %OC between faulty and corresponding normal tests in terms of operating costs is calculated as follows:

$$\%OC = \frac{(OC_{Faulty} - OC_{Baseline})}{OC_{Baseline}} \cdot 100 = \frac{\sum_i UC_{el,i} \cdot P_{el,Faulty,i} \cdot ETS - \sum_i UC_{el,i} \cdot P_{el,Baseline,i} \cdot ETS}{\sum_i UC_{el,i} \cdot P_{el,Baseline,i} \cdot ETS} \cdot 100 \quad (33)$$

where OC_{Faulty} and $OC_{Baseline}$ are, respectively, the operational costs during the faulty test and the corresponding normal experiment, $P_{el,Faulty,i}$ and $P_{el,Baseline,i}$ are, respectively, the electric power demand in the case of the faulty test and the corresponding normal test at the i-th time step, $UC_{el,i}$ is the unit cost of electricity purchased from the grid at the same i-th time step, and ETS is the experimental data acquisition time step (equal to 1 s). The values of $UC_{el,i}$ in Italy depend on the region where electricity is consumed, the day of the year as well as the time of the day. In this study, the comparison has been carried out by assuming that the day of the faulty test coincides with that one of the corresponding normal test. In particular, Fig. 4a and b report the values of $UC_{el,i}$ for each couple of faulty and normal tests under comparison during summer (a) and winter (b) in Aversa. These data are obtained from the company GME Gestore Mercati Energetici S.p.A. [56], an Italian company responsible for the organization and management of the electricity market, as well as ensuring the economic management of adequate availability of energy reserves. The values of the $UC_{el,i}$ reported in Fig. 4 varies from a minimum of 98.56 €/MWh up to a maximum of 512.40 €/MWh.

The values of OC are reported in Table A.4 in Appendix A upon varying the normal/faulty test as well as the AHU component. Table 9 reports the values of %OC upon varying both the pair of tests under comparison and AHU component with reference to the operation of (1) the supply air fan, (2) the return air fan, (3) the refrigerating system and its circulating pump, (4) the heat pump and its circulating pump (5) the steam humidifier as well as (6) the entire AHU during cooling and heating seasons. The cells in Table 9 are filled in yellow if %OC is included in the range ± 10%, in red if %OC is greater than 20% or lower than –20%, in orange in other cases (the symbol N.A. denotes that the AHU component has not been activated during both tests and the calculation of %OC is not possible, while the symbol '∞' indicates that the AHU component has not been activated only during the normal test). According to Table 9, the values of %OC corresponding to the total daily electric demand range from –80.7% up to 82.0%.

Table 8
Values of $\%E_{el}$ (calculated via Eq. (32) as function of both normal/faulty test and AHU component during the summer and winter.

	SAF	RAF	RS + PRS	HP + PHP	HUM	TOTAL
$\%E_{el,SF1\ vs.\ SN2}$ (%)	–0.4	–0.1	4.0	13.2	–100.0	–5.8
$\%E_{el,SF2\ vs.\ SN3}$ (%)	–1.4	–0.2	4.0	–68.7	471.6	31.6
$\%E_{el,SF3\ vs.\ SN4}$ (%)	–1.3	0.0	–12.9	30.6	140.3	12.9
$\%E_{el,SF4\ vs.\ SN2}$ (%)	2.1	–0.4	–28.0	–14.9	–100.0	–30.9
$\%E_{el,SF5\ vs.\ SN1}$ (%)	0.8	–1.2	16.0	–49.0	–100.0	–15.7
$\%E_{el,SF6\ vs.\ SN4}$ (%)	1.1	0.5	10.0	–7.7	40.3	8.1
$\%E_{el,SF7\ vs.\ SN4}$ (%)	3.3	0.8	1.3	–100.0	–100.0	–31.6
$\%E_{el,SF8\ vs.\ SN5}$ (%)	–1.0	–0.8	21.6	86.5	244.1	63.3
$\%E_{el,SF9\ vs.\ SN5}$ (%)	–1.1	–0.9	–84.1	–100.0	–88.7	–80.5
$\%E_{el,SF10\ vs.\ SN5}$ (%)	–3.3	–77.1	–6.8	11.5	–3.6	–3.5
$\%E_{el,SF11\ vs.\ SN6}$ (%)	–72.5	–3.6	–43.8	–98.2	N.A.	–60.1
$\%E_{el,WF1\ vs.\ WN7}$ (%)	0.0	–0.2	1.7	4.2	N.A.	2.5
$\%E_{el,WF2\ vs.\ WN4}$ (%)	–0.2	–1.2	–7.9	–32.3	∞	13.2
$\%E_{el,WF3\ vs.\ WN3}$ (%)	–1.0	0.0	–9.8	41.1	212.0	23.7
$\%E_{el,WF4\ vs.\ WN6}$ (%)	–0.1	0.3	–0.4	–3.1	–100.0	–15.6
$\%E_{el,WF5\ vs.\ WN5}$ (%)	0.8	0.2	9.8	–80.1	–54.5	–22.9
$\%E_{el,WF6\ vs.\ WN8}$ (%)	–0.4	0.1	0.3	6.8	33.9	5.3
$\%E_{el,WF7\ vs.\ WN2}$ (%)	2.4	0.8	–7.3	–94.5	–100.0	–37.8
$\%E_{el,WF8\ vs.\ WN5}$ (%)	–4.4	–0.7	16.9	194.9	196.7	82.8
$\%E_{el,WF9\ vs.\ WN1}$ (%)	1.7	–2.4	–88.0	–80.7	N.A.	–73.6
$\%E_{el,WF10\ vs.\ WN2}$ (%)	–2.3	–77.6	–17.6	23.0	732.3	7.9
$\%E_{el,WF11\ vs.\ WN2}$ (%)	–74.8	–2.9	–29.3	–20.1	–100.0	–31.5

Legend

	$-10\% \le \%E_{el} \le +10\%$
	$+10\% < \%E_{el} \le +20\%$ OR $-20\% \le \%E_{el} < -10\%$
	$\%E_{el} > +20\%$ OR $\%E_{el} < -20\%$

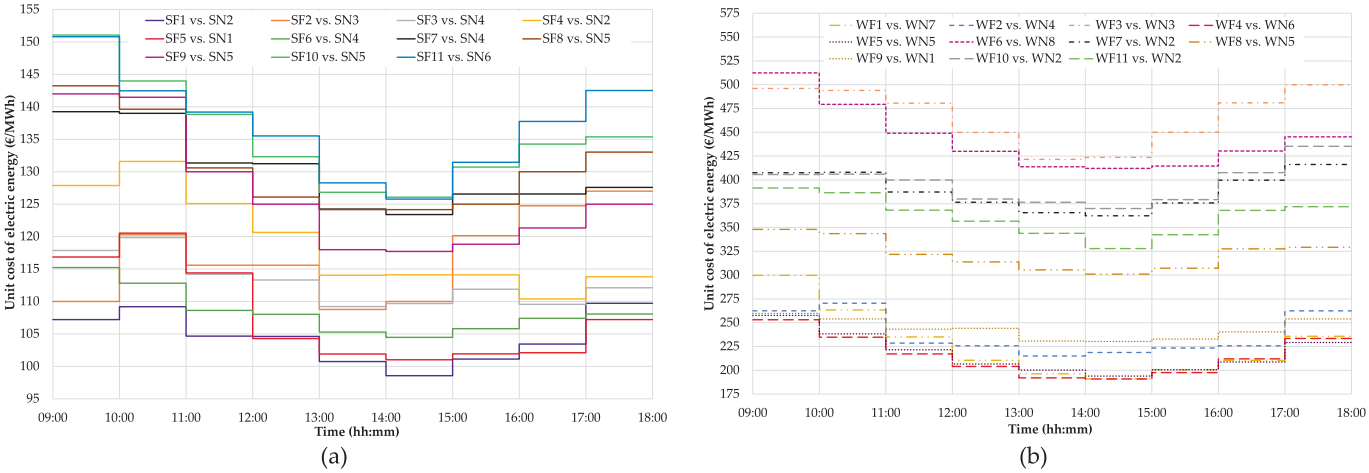


Fig. 4. Values of $UC_{el,i}$ as a function of tests and time during summer (a) and winter (b) in Aversa.

5.5. Effects of faults on global equivalent CO_2 emissions

In this section the effects of the selected faults in terms of daily global equivalent CO_2 emissions are reported. This evaluation is conducted in this study via the energy output-based emission factor approach proposed in [57]. Based on this approach, the mass m_x of a given pollutant x while generating the energy output E can be calculated as:

$$m_x = U_x \cdot E \tag{34}$$

where U_x is the energy output-based emission factor, that is the specific emission of equivalent global pollutant x per unit of E. This approach, although simplified, has been used for assessing the environmental impact in several recent scientific works [31,56,58]. This energy output-based emission factor relies on various operating and structural variables. Among pollutants, CO_2 emissions are generally quantitatively more significant than other GHG emissions [59]. Most scientific papers using this approach adopt a constant CO_2 emission factor over time [31]. In contrast, this study employed a more realistic method by incorporating a time-varying CO_2 emission factor based on actual data. In particular, carbon dioxide emission factor related to the electricity production in Italy $U^{el}_{CO_2}$ relies on the day of the year and the time of the day when electric energy is produced. In this paper, the comparisons between normal and faulty tests have been conducted under the assumption that the day of the faulty test coincides with that one of the associated normal test. Fig. 5 reports the carbon dioxide emission factor associated to the electricity generation in Italy for each pair of corresponding normal and faulty tests upon varying the time during summer (a) and winter (b) in Aversa. These data have been derived from the company Electricity Maps [60], that is specialized in organizing worldwide electricity data to facilitate the transition towards a fully decarbonized electricity system across more than 200 zones globally. According to Fig. 5, the values of $U^{el}_{CO_2}$ change between a minimum of 178.13 gCO_2/kWh and a maximum of 454.11 gCO_2/kWh.

The percentage difference $\%CO_2$ between faulty and normal tests in terms of global equivalent CO_2 emissions is calculated as follows:

$$\%CO_2 = \frac{mCO_{2,Faulty} - mCO_{2,Baseline}}{mCO_{2,Baseline}} \cdot 100 = \frac{\sum_i U^{el}_{CO_2,i} \cdot P_{el,Faulty,i} \cdot ETS - \sum_i U^{el}_{CO_2,i} \cdot P_{el,Baseline,i} \cdot ETS}{\sum_i U^{el}_{CO_2,i} \cdot P_{el,Baseline,i} \cdot ETS} \cdot 100 \tag{35}$$

where $mCO_{2,Faulty}$ and $mCO_{2,Baseline}$ are, respectively, the mass of global equivalent CO_2 emissions of AHU during faulty and corresponding normal test.

The values of $mCO_{2,Faulty}$ and $mCO_{2,Baseline}$ are reported in Table A.5 in Appendix A. Table 10 reports the values of $\%CO_2$ referred to the operation of (1) the supply air fan, (2) the return air fan, (3) the refrigerating system and its circulating pump, (4) the heat pump and its circulating pump (5) the steam humidifier as well as (6) the entire AHU during summer and winter. The cells of Table 10 are filled in yellow if $\%CO_2$ is included in the range ± 10%, in red if $\%CO_2$ is greater than 20% or lower than –20%, in orange in other cases (the symbol N.A. denotes that the AHU component has not been activated during both tests and calculating $\%CO_2$ is not applicable, while the symbol '∞' indicates that the AHU component has not been activated only during the normal test). According to Table 10, the values of $\%CO_2$ corresponding to the total daily electric demand range from –80.6% up to 85.1%.

While the environmental assessment performed in this work focuses on global equivalent CO_2 emissions associated to operational energy demands, it should be underlined that it does not capture the broader carbon impacts associated with component degradation and replacement (that are not reflected in energy consumption, but can significantly contribute to the building's overall environmental footprint). This aspect is particularly important in the case of hard faults, which, differently from soft faults that can often be resolved by adjusting the control logic, involve actual component failures that require physical replacement introducing additional embodied emissions related to manufacturing, transport, and disposal.

5.6. Effects of faults on operation time of AHU components

In this section the effects of the selected faults in terms of daily operation time of AHU components are described. Table 11 reports the percentage of difference %OT between faulty and corresponding normal tests in terms of operation time with reference to the operation of (1) the supply air fan, (2) the return air fan, (3) the refrigerating system (4), the heat pump (5), the steam humidifier, (6) the circulating pump of the refrigerating system, and (7) the circulating pump of the heat pump during summer and winter. Th values of %OT are calculated as follows:

$$\%OT = \frac{(OT_{Faulty} - OT_{Baseline})}{OT_{Baseline}} \cdot 100 \tag{36}$$

where OT_{Faulty} and $OT_{Baseline}$ are, respectively, the operating time during faulty and corresponding normal test. The cells of Table 11 are filled in yellow if %OT is included in the range ± 10%, in red if %OT is greater than 20% or lower than –20%, in orange in other cases (the symbol N.A. denotes that the AHU component has not been activated during both tests, while the symbol '∞' indicates that the AHU component has not been activated only during the normal test). The values of $OT_{Baseline}$ and OT_{Faulty} are reported in Table A.6 in Appendix A upon varying both the normal/faulty test and AHU component.

Table 9
Values of %OC (calculated via Eq. (33) as a function of both pairs of tests under comparison and AHU component during summer and winter.

	SAF	RAF	RS + PRS	HP + PHP	HUM	TOTAL
$\%OC_{SF1\ vs.\ SN2}$ (%)	–0.4	–0.1	4.0	13.1	–100.0	–5.9
$\%OC_{SF2\ vs.\ SN3}$ (%)	–1.5	–0.2	4.2	–68.9	465.0	31.7
$\%OC_{SF3\ vs.\ SN4}$ (%)	–1.3	0.0	–12.8	30.5	140.3	13.0
$\%OC_{SF4\ vs.\ SN2}$ (%)	2.1	–0.4	–27.8	–14.5	–100.0	–30.7
$\%OC_{SF5\ vs.\ SN1}$ (%)	0.8	–1.2	16.3	–50.3	–100.0	–15.7
$\%OC_{SF6\ vs.\ SN4}$ (%)	1.1	0.5	10.2	–8.2	38.6	7.9
$\%OC_{SF7\ vs.\ SN4}$ (%)	3.4	0.7	1.5	–100.0	–100.0	–31.6
$\%OC_{SF8\ vs.\ SN5}$ (%)	–1.0	–0.7	21.4	86.9	241.3	62.8
$\%OC_{SF9\ vs.\ SN5}$ (%)	–1.0	–0.8	–84.2	–100.0	–89.7	–80.7
$\%OC_{SF10\ vs.\ SN5}$ (%)	–3.3	–77.1	–7.2	11.5	–2.7	–3.6
$\%OC_{SF11\ vs.\ SN6}$ (%)	–72.5	–3.6	–43.7	–98.1	N.A.	–60.0
$\%OC_{WF1\ vs.\ WN7}$ (%)	0.0	–0.3	2.9	4.2	N.A.	3.1
$\%OC_{WF2\ vs.\ WN4}$ (%)	–0.2	–1.2	–8.1	–32.9	∞	12.7
$\%OC_{WF3\ vs.\ WN4}$ (%)	–1.0	0.0	–9.7	40.8	210.5	23.6
$\%OC_{WF4\ vs.\ WN6}$ (%)	–0.1	0.3	–0.6	–2.6	–100.0	–15.3
$\%OC_{WF5\ vs.\ WN5}$ (%)	0.9	0.1	9.4	–80.0	–57.7	–23.8
$\%OC_{WF6\ vs.\ WN8}$ (%)	–0.4	0.1	0.3	7.3	34.3	5.5
$\%OC_{WF7\ vs.\ WN2}$ (%)	2.4	0.8	–7.3	–94.4	–100.0	–37.9
$\%OC_{WF8\ vs.\ WN5}$ (%)	–4.4	–0.7	16.6	192.3	193.8	82.0
$\%OC_{WF9\ vs.\ WN1}$ (%)	1.7	–2.4	–87.9	–80.4	N.A.	–73.5
$\%OC_{WF10\ vs.\ WN2}$ (%)	–2.3	–77.6	–17.8	23.5	665.1	7.9
$\%OC_{WF11\ vs.\ WN2}$ (%)	–74.8	–2.9	–29.3	–19.5	–100.0	–31.3

Legend

	–10% ≤ %OC ≤ +10%
	+10% < %OC ≤ +20% OR –20% ≤ %OC < –10%
	%OC > +20% OR %OC < –20%

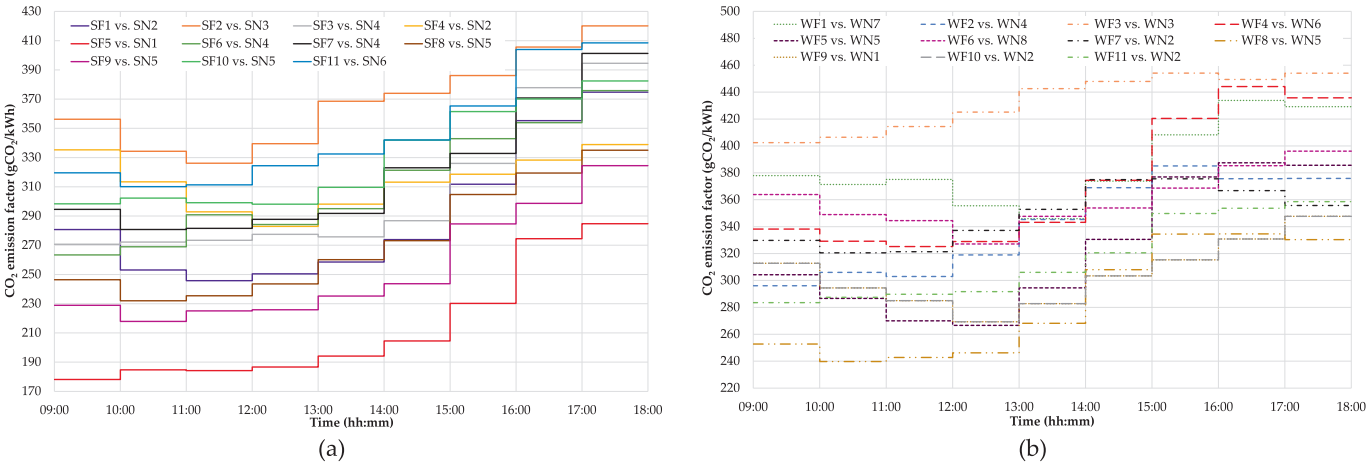


Fig. 5. CO_2 emission factor associated to electricity consumption as a function of the time during summer (a) and winter (b) in Aversa.

5.7. Discussions of faults' impacts

This section discusses the impacts of the investigated faults from multiple perspectives to provide a comprehensive understanding of their consequences. Subsection 5.7.1 examines the influence of faults on indoor thermo-hygrometric conditions. Subsection 5.7.2 analyzes the effects of faults on electrical power consumption. Finally, subsection 5.7.3 explores the broader implications of these faults in terms of total daily energy consumption, operational costs, global equivalent CO_2 emissions, and operating time of AHU components.

5.7.1. Analysis of faults impacts in term of indoor thermo-hygrometric conditions

According to Table 5, fault 1 has a strong negative impact on indoor relative humidity met ratio only during summer (RHMR is strongly reduced from 92.2% in the case of normal test down to 25.4% for the faulty experiment), together with a worst value of $|\bar{\varepsilon}_{RH,D}|$(increases from 1.8% during the normal test up to 2.2% in the case of the faulty test). This fault has a negative effect also based on the data reported in Table 6, where a significant increase of the value of dRH_{tot} during summer by about 1068% can be recognized. These results are due to the fact that the return air relative humidity sensor is providing wrong readings (i.e., 15% larger than the real return air relative humidity values).

Table 5 indicates that fault 2 results in a significant decrease in terms of indoor air relative humidity met ratio during both winter (where RHMR becomes equal to 0.0% during the faulty experiment) and summer (where RHMR becomes equal to 0.6% during the faulty test), together with a much higher relevance of deviations from desired indoor air relative humidity during both summer ($|\bar{\varepsilon}_{RH,D}|$ rises from 2.5% during the normal test up to 11.9% in the case of the faulty test) and winter ($|\bar{\varepsilon}_{RH,D}|$ increases from 1.4% during the normal test up to 8.7% in the case of the faulty test). According to Table 6, this fault significantly increases the values of dRH_{max} and dRH_{tot}, respectively, by about 200% and 4547% during summer as well as by around 284% and 6605% during winter. The above-mentioned outputs are caused by the fact that the return air relative humidity sensor is reading values that are 15% lower than the real return air relative humidity values.

Fault 5 results in a significant reduction in terms of indoor air temperature met ratio during both summer (TMR is notably decreased from 68.8% in the case of normal experiment down to 2.5% for the faulty experiment) and winter (TMR is strongly reduced from 78.2% in the case of normal test down to 0.0% for the faulty test); in addition, a worst relevance of deviations from desired indoor air temperature is also obtained during both summer ($|\bar{\varepsilon}_{T,D}|$ rises from 0.3 °C during the normal test up to 1.9 °C in the case of the faulty test) and winter ($|\bar{\varepsilon}_{T,D}|$ increases from 0.5 °C during the normal experiment up to 1.6 °C in the case of the faulty experiment). As reported in Table 6, this fault also causes a significant increase of both dT_{max} and dT_{tot} during both summer (by about 169% and 1844%, respectively) and winter (by approximately by 75% and 1328%, respectively). These data are a consequence of the fact that the return air temperature sensor is providing readings that are 3 °C higher than the real return air temperature values.

As indicated in Table 5, fault 3 significantly reduces indoor air temperature met ratio during both summer (TMR is strongly reduced from 74.8% in the case of normal test down to 0.0% for the faulty experiment) and winter (TMR is notably decreased from 75.2% in the case of normal test down to 8.2% for the faulty experiment); in addition, a worst relevance of deviations from desired indoor air temperature is also obtained during both summer ($|\bar{\varepsilon}_{T,D}|$ rises from 0.3 °C during the normal test up to 2.1 °C in the case of the faulty test) and winter ($|\bar{\varepsilon}_{T,D}|$ increases from 0.2 °C during the normal experiment up to 1.9 °C in the case of the faulty experiment). Also, RMHR is negatively impacted by this fault during both summer and winter. According to Table 6, fault 3 also increases the values of dT_{max}, dT_{tot} and dRH_{tot}, respectively, by about 204%, 2686% and 175% during summer tests and by approximately 253%, 3937% and 129% during winter. The above-mentioned outcomes are due to the fact that the return air temperature sensor is reading values that are reduced by 3 °C with respect to the real return air temperatures.

Table 5 indicates that fault 4 significantly reduces indoor air relative humidity met ratio only during winter (RHMR is strongly reduced from 90.9% in the case of normal test down to 18.4% for the faulty experiment), together with a worst value of $|\bar{\varepsilon}_{RH,D}|$(it rises from 0.9% during the normal test up to 2.6% in the case of the faulty test). This fault is characterized by a negative effect also according to the data indicated in Table 6, where a significant increase of dRH_{max} and dRH_{tot}, respectively, by about 55% and 2503% can be recognized during winter only. During summer, the impact of the fault is less significant because the outdoor air has a much higher absolute humidity compared to winter conditions. As a result, the AHU can still compensate for the fault even without the operation of the humidifier.

According to the data in Table 5, it can be underlined that, in the case of fault 9, indoor air temperature met ratio is significantly reduced during both cooling season (TMR is notably reduced from 69.4% in the case of normal experiment down to 1.9% for the faulty experiment) and heating season (TMR is significantly decreased from 76.9% in the case of normal test down to 18.5% for the faulty test); furthermore, a worst relevance of deviations from desired indoor air temperature is also obtained during both cooling season ($|\bar{\varepsilon}_{T,D}|$ increases from 0.3 °C during

Table 10
Values of $\%CO_2$ (calculated via Eq. (35) as a function of both pairs of tests under comparison and AHU component during summer and winter.

	SAF	RAF	RS + PRS	HP + PHP	HUM	TOTAL
$\%CO_{2,SF1\ vs.\ SN2}$ (%)	–0.4	–0.1	3.7	13.5	–100.0	–5.9
$\%CO_{2,SF2\ vs.\ SN3}$ (%)	–1.6	–0.2	4.2	–68.7	464.3	31.7
$\%CO_{2,SF3\ vs.\ SN4}$ (%)	–1.2	0.0	–13.6	30.9	139.2	12.5
$\%CO_{2,SF4\ vs.\ SN2}$ (%)	2.1	–0.4	–27.8	–14.5	–100.0	–30.7
$\%CO_{2,SF5\ vs.\ SN1}$ (%)	0.8	–1.1	15.7	–47.0	–100.0	–15.8
$\%CO_{2,SF6\ vs.\ SN4}$ (%)	1.0	0.5	9.7	–6.2	44.5	8.7
$\%CO_{2,SF7\ vs.\ SN4}$ (%)	3.2	0.8	0.8	–100.0	–100.0	–31.8
$\%CO_{2,SF8\ vs.\ SN5}$ (%)	–1.0	–0.8	21.9	85.5	250.8	64.2
$\%CO_{2,SF9\ vs.\ SN5}$ (%)	–1.1	–1.0	–84.0	–100.0	–89.2	–80.6
$\%CO_{2,SF10\ vs.\ SN5}$ (%)	–3.3	–77.1	–6.0	12.7	–7.2	–3.3
$\%CO_{2,SF11\ vs.\ SN6}$ (%)	–72.4	–3.6	–43.7	–98.4	N.A.	–60.0
$\%CO_{2,WF1\ vs.\ WN7}$ (%)	0.0	–0.3	1.7	4.1	N.A.	2.5
$\%CO_{2,WF2\ vs.\ WN4}$ (%)	–0.2	–1.1	–7.7	–31.4	∞	13.6
$\%CO_{2,WF3\ vs.\ WN3}$ (%)	–1.0	0.0	–10.0	41.0	208.6	23.6
$\%CO_{2,WF4\ vs.\ WN6}$ (%)	–0.1	0.2	–0.6	–4.3	–100.0	–16.2
$\%CO_{2,WF5\ vs.\ WN5}$ (%)	0.8	0.2	10.9	–79.9	–51.4	–22.1
$\%CO_{2,WF6\ vs.\ WN8}$ (%)	–0.4	0.1	0.2	6.6	31.8	5.1
$\%CO_{2,WF7\ vs.\ WN2}$ (%)	2.4	0.8	–7.2	–94.4	–100.0	–37.7
$\%CO_{2,WF8\ vs.\ WN5}$ (%)	–4.5	–0.7	17.7	196.7	206.5	85.1
$\%CO_{2,WF9\ vs.\ WN1}$ (%)	1.7	–2.4	–88.0	–80.5	N.A.	–73.6
$\%CO_{2,WF10\ vs.\ WN2}$ (%)	–2.3	–77.6	–17.6	23.2	624.8	7.8
$\%CO_{2,WF11\ vs.\ WN2}$ (%)	–74.8	–2.9	–29.1	–24.5	–100.0	–33.1

Legend

	$-10\% \le \%CO_2 \le +10\%$
	$+10\% < \%CO_2 \le +20\%$ OR $-20\% \le \%CO_2 < -10\%$
	$\%CO_2 > +20\%$ OR $\%CO_2 < -20\%$

the normal test up to 2.0 °C in the case of the faulty test) and heating season ($|\bar{\varepsilon}_{T,D}|$ rises from 0.2 °C during the normal experiment up to 0.6 °C in the case of the faulty experiment). The above-mentioned results are linked to the fact that it is not possible to reduce return air temperature by using the refrigeration system due to the fault occurrence. Indoor air relative humidity met ratio is also negatively impacted by this fault during cooling season due to the fact that dehumidification is not allowed because of the cooling coil valve is closed. Based on Table 6, the values of dT_{max}, dT_{tot} and dRH_{tot} are remarkably increased, respectively, by about 169%, 1897%, and 204% during summer; during winter dT_{tot} and dRH_{max} increase, respectively, by around 1065% and about 22%.

Table 5 highlights that fault 6 has no significant effect on indoor air temperature and relative humidity met ratios during both seasons because during both summer and winter the cooling coil valve is open for the majority (more than 90%) of the corresponding normal tests' durations and, therefore, the difference with respect to the faulty scenarios is not relevant. With reference to the data in Table 6, it can be underlined that the fault 6 increases dT_{max} by around 34% during summer, while during winter this fault leads to an increase of dRH_{max} and dRH_{tot}, respectively, by around 63% and 37%.

As indicated in Table 5, fault 7 results in a significant reduction in terms of indoor air temperature met ratio during both summer (TMR is notably decreased from 74.8% in the case of normal experiment down to 2.6% for the faulty experiment) and winter (TMR is strongly reduced from 75.8% in the case of normal test down to 0.0% for the faulty test); in addition, a worst relevance of deviations from desired indoor air temperature is also obtained during both summer ($|\bar{\varepsilon}_{T,D}|$ increases from 0.3 °C during the normal test up to 3.8 °C in the case of the faulty test) and winter ($|\bar{\varepsilon}_{T,D}|$ rises from 0.2 °C during the normal experiment up to 3.0 °C in the case of the faulty experiment). Indoor air relative humidity met ratio is also negatively impacted by this fault during both summer (where RHMR is strongly decreased from 91.8% in the case of normal experiment down to 57.8% during the faulty experiment) and winter (where RHMR is notably reduced from 96.8% in the case of normal experiment down to 0.0% during the faulty test), together with a higher relevance of deviations from desired indoor air relative humidity during both summer ($|\bar{\varepsilon}_{RH,D}|$ increases from 2.0% during the normal test up to 2.5% in the case of the faulty test) and winter ($|\bar{\varepsilon}_{RH,D}|$ rises from 1.2% during the normal test up to 2.9% in the case of the faulty test). Table 6 indicates that this fault significantly increases the values of dT_{max}, dT_{tot} and dRH_{tot}, respectively, by about 409%, 4779% and 554% during summer as well as by around 377%, 7270% and 7347% during winter. All the above-mentioned effects are due to the fact that the utilization of the post-heating coil is not possible due to the fault occurrence.

In the case of fault 8, Table 5 shows that there is a relevant decrease of indoor air temperature met ratio during both summer (TMR is notably decreased from 69.4% in the case of normal experiment down to 0.0% for the faulty experiment) and winter (TMR is strongly reduced from 78.2% in the case of normal test down to 5.5% for the faulty test); in addition, a worst relevance of deviations from desired indoor air temperature is also obtained during both summer ($|\bar{\varepsilon}_{T,D}|$ increases from 0.3 °C during the normal test up to 2.5 °C in the case of the faulty test) and winter ($|\bar{\varepsilon}_{T,D}|$ rises from 0.5 °C during the normal experiment up to 3.9 °C in the case of the faulty experiment). The values of dT_{max} and dT_{tot} increase notably during summer (by 149% and 2403%, respectively), while during winter the values of dT_{max}, dT_{tot} dRH_{max} and dRH_{tot} are enhanced by 361%, 3079%, 50% and 63%, respectively. These effects are due to the facts that (i) the post-heating coil is used for a limited period during the summer and winter normal experiments, while (ii) the cooling coil valve is open for the most part of the corresponding normal tests (for cooling and/or dehumidification purposes) during both summer and winter and, therefore, the cooling coil operation cannot compensate the prolonged operation of the PostHC due to the fault occurrence;

Fault 10 has minimal effects on both indoor air temperature and relative humidity met ratios (according to Table 5), but it increases mainly during winter the relevance of deviations from both desired indoor air temperature ($|\bar{\varepsilon}_{T,D}|$ rises from 0.2 °C during the normal test up to 0.3 °C in the case of the faulty test) and desired indoor air humidity ($|\bar{\varepsilon}_{RH,D}|$ increases from 1.2% during the normal test up to 2.5% in the case of the faulty test). These effects are justified taking into account that the complete failure of the return air fan is compensated by the operation of the supply return air fan.

During summer fault 11 leads to an important reduction of both indoor air temperature met ratio (TMR is strongly reduced from 77.3% in the case of normal test down to 58.7% for the faulty experiment) and indoor air relative humidity met ratio (RHMR is strongly reduced from 93.3% in the case of normal test down to 31.3% for the faulty experiment). As indicated in Table 6, it also causes a significant increase of dT_{tot} and dRH_{tot} by about 161% and 229%, respectively, during summer; these results are because of the RS cannot reduce return air temperature down to the lower deadband (staring from the initial indoor air conditions of the faulty experiment). During winter the differences between faulty and normal tests in terms of TMR and RHMR are irrelevant thanks to the fact that the HP is able to increase the initial values of T_{RA} and keep them within the defined deadbands (even with low supply air flowrate).

The worst TMR value (0%) is obtained in the case of the faults 3 and 8 during the summer, as well as in the case of the faults 5 and 7 during the winter. The value of TMR = 0% during the test SF3 is linked to the fact that the return air temperature sensor reads an incorrect value that is always 3 °C lower than the actual value, so the control logic does not activate the AHU cooling coil for cooling purposes. In the case of the test SF8, the TMR value of 0% is due to the fact that the heating coil is always active, which balances the operation of the cooling coil and does not allow the desired cooling of indoor air. The value of TMR equal to 0% during the test WF5 is linked to the fact that the return air temperature sensor reads an incorrect value that is always 3 °C higher than the actual value, so the hot coil is not activated. In the case of the test WF7, the value of 0% for TMR is associated to the fact that the heating coil is always deactivated, so it is not possible to achieve the desired heating of indoor air. The worst RHMR value (0%) is obtained with reference to the faults 2 and 7 during winter. The value of RHMR of 0% during the test WF2 test is related to the fact that the return air relative humidity sensor reads an incorrect value that is always 15% lower than the actual value, so the AHU control logic does not activate the cooling coil for dehumidification. During the WF7 test, RHMR assumes a value of 0% because, on the one hand, the return air temperature is always lower than the relative lower deadband (19 °C), so the cooling coil is not activated for its control; on the other hand, the return air relative humidity is always higher than the corresponding upper deadband (55%), so it would be necessary to activate the cooling coil to dehumidify; there are, therefore, two conflicting requirements, and the AHU logic prioritizes the control of the return air temperature (rather than the relative humidity), so it does not activate the cooling coil; as a consequence, the relative humidity of the return air always remains above 55%.

5.7.2. *Analysis of faults impacts in terms of electric power demand*

Table 7, Table A.2 of Appendix A and Fig. 3 show the following main outcomes:

- fault 1 does not have a significant impact on electrical power consumption of AHU components during both winter and summer with the exception of the humidifier under summer conditions, which results in a reduction of about 19% in terms of peak power (due to the fact that during the faulty experiment SF1 the humidifier is never turned on, as indicated in Tables 11 and A.6);
- fault 2 determines an increase of the mean of electrical power consumption of the refrigeration system, the heat pump, and the

Table 11
Values of %OT (calculated via Eq. (36) as a function of pairs of tests under comparison and AHU component during summer and winter.

	SAF	RAF	RS	HP	HUM	PRS	PHP
$\%OT_{SF1\ vs.\ SN2}$ (%)	0.0	0.0	2.9	17.9	–100.0	11.5	8.8
$\%OT_{SF2\ vs.\ SN3}$ (%)	–0.1	–0.1	–8.3	–77.0	420.5	–0.2	–65.1
$\%OT_{SF3\ vs.\ SN4}$ (%)	0.0	0.0	–8.9	25.4	140.2	–24.0	39.3
$\%OT_{SF4\ vs.\ SN2}$ (%)	–0.2	–0.1	–42.8	–45.0	–100.0	–32.7	–10.6
$\%OT_{SF5\ vs.\ SN1}$ (%)	–0.2	0.0	–20.1	–63.9	–100.0	24.3	–54.2
$\%OT_{SF6\ vs.\ SN4}$ (%)	0.0	0.0	10.3	–6.1	38.3	10.6	–8.4
$\%OT_{SF7\ vs.\ SN4}$ (%)	0.0	0.0	–1.5	–100.0	–100.0	10.2	–100.0
$\%OT_{SF8\ vs.\ SN5}$ (%)	0.0	0.0	20.0	83.8	226.0	22.2	89.4
$\%OT_{SF9\ vs.\ SN5}$ (%)	0.0	0.0	–79.5	–100.0	–88.1	–100.0	–100.0
$\%OT_{SF10\ vs.\ SN5}$ (%)	0.0	–100.0	–10.7	11.4	–4.6	1.7	13.0
$\%OT_{SF11\ vs.\ SN6}$ (%)	–100.0	0.0	–62.0	–97.2	N.A.	0.0	–100.0
$\%OT_{WF1\ vs.\ WN7}$ (%)	0.0	0.0	2.9	3.3	N.A.	0.0	4.5
$\%OT_{WF2\ vs.\ WN4}$ (%)	0.0	0.0	2.2	–34.5	∞	–18.9	–28.2
$\%OT_{WF3\ vs.\ WN3}$ (%)	0.0	0.0	–0.6	36.0	193.6	–17.6	53.1
$\%OT_{WF4\ vs.\ WN6}$ (%)	0.0	0.0	1.5	–3.2	–100.0	–2.6	–2.7
$\%OT_{WF5\ vs.\ WN5}$ (%)	0.1	0.0	11.9	–75.4	–51.9	7.4	–100.0
$\%OT_{WF6\ vs.\ WN8}$ (%)	0.0	0.0	–10.7	7.6	32.6	0.5	4.8
$\%OT_{WF7\ vs.\ WN2}$ (%)	0.0	0.0	–13.8	–92.2	–100.0	–0.1	–100.0
$\%OT_{WF8\ vs.\ WN5}$ (%)	0.0	0.0	26.4	161.4	184.2	7.5	400.4
$\%OT_{WF9\ vs.\ WN1}$ (%)	0.2	0.0	–73.0	–76.5	N.A.	–100.0	–91.4
$\%OT_{WF10\ vs.\ WN2}$ (%)	0.0	–100.0	–29.3	20.9	640.6	–5.6	27.7
$\%OT_{WF11\ vs.\ WN2}$ (%)	–100.0	0.0	–58.5	–54.2	–100.0	–0.1	58.8

Legend

	–10% ≤ %OT ≤ +10%
	+10% < %OT ≤ +20% OR –20% ≤ %OT < –10%
	%OT> +20% OR %OT < –20%

humidifier by about 15%, 23% and 10%, respectively, while the standard deviation of electrical power consumption is significantly impacted, whatever the AHU component is. During winter, this fault has negligible effects on both $\%\mu_{el}$ and $\%\sigma_{el}$ with reference to all AHU components, except the humidifier (that is never operated during the normal winter test WN4) causing an increase of peak power by around 25% due to the fact that the humidifier is activated for a longer period (as reported in Tables 11 and A.6);

- during summer fault 5 determines a reduction of both $\%\mu_{el}$ and $\%\sigma_{el}$ for the humidifier by 100% with respect to the summer normal test SN1. On the other hand, during summer the RS and the HP increase their mean electrical power consumption, respectively, by about 41% and 52%, with the values of $\%\sigma_{el}$ strongly impacted for almost all the AHU components. During winter the values of $\%\mu_{el}$ are not significantly affected by the fault 5 with reference to all the AHU components. Peak power (as indicated in Fig. 3) is significantly reduced during summer and winter, respectively, by about –15% and –23% thanks to the fact that the operation of both the HP (and its circulating pump) and the humidifier are strongly reduced (as indicated in Tables 11 and A.6);
- fault 3 does not cause a significant variation in terms of mean and standard deviation of electrical power consumption of AHU components during summer, while during winter only the return air fan ($\%\sigma_{el}$ equal to about –42%) and the humidifier ($\%\sigma_{el}$ of about –21%) are affected. Peak power is impacted solely during the winter test, showing a decrease of about –17% thanks to the fact that the operation of the RS (and related PRS) is reduced (as reported in Tables 11 and A.6);
- faulty 4 clearly affects the operation of the humidifier during both summer and winter (both $\%\mu_{el}$ and $\%\sigma_{el}$ are equal to –100%). In addition, this fault causes an increase of the mean of electrical power consumption associated to the RS and the HP by about 29% and 49%, respectively, during summer; the values of $\%\sigma_{el}$ are notably affected during summer, whatever the AHU component is. Peak power is impacted during both summer and winter, with a reduction of approximately 18% during both seasons in the case of faulty scenarios;
- fault 9 has a negligible influence on the mean electrical power consumption of the AHU components with respect to the normal operation during both seasons, except the HP (and related PHP) that is not operated during the summer faulty test SF9 (thanks to the missing operation of the RS and related PRS). Peak power is notably decreased by about –61% during summer mainly thanks to the reduced activation of both the RS and HP (and their circulating pumps);
- fault 6 has a negligible influence on $\%\mu_{el}$, except for the refrigeration system during winter (with a small increase of $\%\mu_{el}$ by about 13%); peak power is only affected during winter, with an increase of about 27%; these outcomes depend on the fact that during summer and winter the cooling coil valve is open for the majority (more than 90%) of the corresponding normal tests' durations and, therefore, the difference with respect to the faulty scenarios is not relevant.
- fault 7 is characterized by a not relevant effect on the values of $\%\mu_{el}$, except the heat pump and the humidifier (due to the fact that the humidifier is not operated during both summer and winter, while the HP is not activated during summer only). This results in a signification reduction by about –57% in terms of peak power value during summer thanks to the lower operation time of both the humidifier and the heat pump;
- fault 8 does not determine a significant variation in terms of mean electrical power consumption of the AHU components and overall peak power during both summer and winter;
- fault 10 reduces the mean and the standard deviation of electrical power consumption of the return air fan itself by about 77% and 98%, respectively, during both summer and winter. The electric motor of this fan is characterized by a minimum electrical power consumption (different from zero) even in the case of failure due to the fact that this fault is artificially implemented in this study by forcing the control signal (instead of applying a physical stuck of the RAF motor). In addition, during winter the humidifier increases its mean electrical power consumption by about 12%, while the standard deviation of its electrical power consumption reduces by about 36%; this is due to that fact that this fault enhances the outside air flowrate (characterized by lower humidity ratio in comparison to the return air), thus requiring a longer operation of the humidifier (as indicated in Tables 11 and A.6). This leads to a larger overall peak power by about 22% during winter;
- fault 11 has a significant impact on the mean and standard deviation of electrical power consumption of the supply air fan itself, which are reduced, respectively, by about 73% and 67%, during summer and around 75% and 90% during winter. The electric motor of the fan is characterised by a minimum electrical power consumption (different from zero) due to the fact that the failure of the SAF is not implemented by modifying the control signal, but through a physical stuck of the fan. Moreover, due to the fact that the humidifier is not operated during the winter faulty test, the values of both $\%\mu_{el}$ and $\%\sigma_{el}$ are equal to –100%. Peak power is solely impacted during summer, with a reduction of around –48%.

5.7.3. *Analysis of faults impacts in terms of daily electric energy demand, operating costs, global equivalent CO_2 emissions and operating time of AHU components*

Tables 8-11 and Tables A.3-A.6 of Appendix A indicate the following main effects:

- fault 1 does not have a significant impact on daily electrical energy consumption, global equivalent CO_2 emissions and operation costs of the AHU components during both seasons, with the exception of the humidifier during summer (in the case of the faulty summer experiment SF1 the humidifier is never turned on). These results are due to the fact that during summer the return air relative humidity sensor is providing wrong readings (i.e., 15% larger than the real return air relative humidity values) and, therefore, the humidifier is not activated, while the operation of the PRS is enhanced (in order to dehumidify) and the HP (together with its circulating pump) is also used for a longer time in order to balance the prolonged activation of the PRS (as indicated in Tables 11 and A.6);
- fault 2 determines a relevant decrease of E_{el}, OC and mCO_2 of the heat pump and its related circulating pump with respect to the normal operation during both summer (by about –69%) and winter (by approximately –31 ÷ –33%). As a matter of fact, the HP is operated during summer and winter faulty tests for at least 30 min less than the corresponding normal experiments (as reported in Table A.6 of Appendix A). On the other hand, this fault causes a significant increase of daily electrical energy consumption, operational costs and global equivalent CO_2 emissions of the humidifier during both summer (by about 464 ÷ 472%) and winter (the humidifier is operated during the winter faulty test WF2, while it is not activated during the corresponding winter normal experiment WN4). The differences in terms of total E_{el}, OC and mCO_2 during summer and winter, respectively, are around 32% and about 13 ÷ 14%. The above-mentioned outputs are caused by the fact that the return air relative humidity sensor is reading values that are 15% lower than the real RH_{RA} values; this causes the humidifier to be activated for a longer period, while the operation time of the HP (and its circulating pump) is strongly reduced (as reported in Tables 11 and A.6);
- fault 5 reduces the daily electrical energy consumption, operational costs and global equivalent CO_2 emissions of the HP and its circulating pump by about 49%, 50% and 47%, respectively, during summer and by about 80% during winter. A reduction of E_{el}, OC and mCO_2 is recognized also for the humidifier during both summer (by –100%) and winter (by around –51%÷–58%), while the RS and its

circulating pump increase their daily electrical energy consumption, operation costs and global equivalent CO_2 emissions by about 16% during summer and by around 9%÷11% during winter. The differences between the faulty and normal tests in terms of total E_{el}, OC and mCO_2 are about –16% during summer and around –22%÷–24% during winter. However, these reductions correspond to worst indoor thermal conditions during both summer and winter; in particular, during summer TMR is notably decreased in the case of faulty test in comparison to the corresponding normal test (as reported in Table 5); in addition, a worst relevance of deviations from desired indoor air temperature is also recognized during both heating and cooling seasons (as indicated in Table 5); moreover, during the summer faulty test SF5 also the indoor air relative humidity met ratio is significantly reduced with respect to the corresponding normal test (see Table 5). These data are a consequence of the fact that the return air temperature sensor is providing readings that are 3 °C higher than the real T_{RA} values, so that the operation of both the HP (and its circulating pump) and the humidifier are strongly reduced, while the utilization of the PRS is significantly enhanced (as indicated in Tables 11 and A.6);

- fault 3 leads to an increase of the daily electrical energy consumption, operation costs and global equivalent CO_2 emissions of the heat pump and its related circulating pump by about 31% during summer and by around 41% during winter. A similar effect is observed for the humidifier, while the refrigeration system and its circulating pump are characterized by values of E_{el}, OC and mCO_2 lower than the normal case by about 13%÷14% during summer and by about 10% during winter. The differences between normal and faulty tests in terms of total daily energy consumption, operating costs, and global equivalent CO_2 emissions during summer and winter, respectively, are about 12%÷13% and 24%. The above-mentioned outcomes are due to the fact that the return air temperature sensor is reading values that are reduced by 3 °C with respect to the real values of T_{RA}; this causes the HP (and related circulating pump) to operate for a longer period; in addition, the activation of the humidifier is strongly enhanced, while the operation of the RS (and related PRS) is reduced (as reported in Tables 11 and A.6);
- fault 4 obviously causes values of $\%E_{el}$, %OC and $\%CO_2$ equal to –100% during both summer and winter, for the humidifier itself. In addition, during summer the daily electrical energy consumption, global equivalent CO_2 emissions and operational costs are reduced by about 28% for the refrigeration system (with its circulating pump) thanks to the lower operating time of the humidifier (as reported in Tables 11 and A.6) and by around 15% with reference to the heat pump (with its circulating pump) thanks to the lower operating time of the refrigeration system (as indicated in Tables 11 and A.6). The differences between faulty and normal tests in terms of total E_{el}, OC and mCO_2 are about –31% during summer and around –15%÷–16% during winter. On the other hand, it should be highlighted that, from the point of view of indoor air hygrometric conditions, during the winter faulty test WF4 there is a huge reduction of RHMR in comparison to the normal test WN6 (as reported in Table 5), together with a worst value of $|\bar{\varepsilon}_{RH,D}|$ (as indicated in Table 5);
- fault 9 leads to a significant reduction of the daily electrical energy consumption, operation costs as well as global equivalent CO_2 emissions of the heat pump and the refrigeration system (together with their circulating pumps) by 100% and 84%, respectively, during summer and by around 80%÷81% and 88%, respectively, during winter. For what is concerned the humidifier, its E_{el}, OC and mCO_2 during the summer faulty test SF9 are significantly lower than the corresponding normal case. The differences between faulty and normal tests in terms of total daily energy consumption, operating costs, and global equivalent CO_2 emissions are about –81% during summer and around –74% during winter. These effects are obtained thanks to the fact that, as reported in Tables 11 and A.6, the occurrence of this fault causes a reduced operation time of both the RS and the HP (as well as their circulating pumps). However, this decrease in terms of total E_{el}, OC and mCO_2 is counterbalanced by a relevant reduction of indoor air temperature met ratio during both cooling season and heating season (as reported in Table 5); furthermore, a worst relevance of deviations from desired indoor air temperature is also recognized during both summer and winter (as indicated in Table 5);
- whatever the season is, fault 6 has a negligible influence in terms of daily electric energy consumption, operating costs, and global equivalent CO_2 emissions on the operation of the AHU components in comparison to the normal operation, with the exception of the humidifier and the refrigeration system. The differences between faulty and normal tests in terms of total E_{el}, OC and mCO_2, respectively, are approximately 8%÷9% during summer and around 5% during winter. These outcomes depend on the fact that during the normal tests the cooling coil valve is fully open during the most part of time (about 90% during the summer normal test SN4 and around 99% during the winter normal test WN8) for cooling and/or dehumidification purposes;
- fault 7 significantly reduces the daily electrical energy consumption, operating costs as well as global equivalent CO_2 emissions of both the humidifier (by 100% during both summer and winter) and the heat pump (with its circulating pump) by 100% during summer and by about 94% during winter. The differences between faulty and normal tests in terms of total E_{el}, OC and mCO_2 are around –32% during summer and about –38% during winter. These results are mainly because the utilization of the PostHC is not allowed and, therefore, the operation time of both the HP and related circulating pump are strongly reduced (as reported in Tables 11 and A.6); also the energy demand of the humidifier is lowered. These reductions are counterbalanced by the fact that this fault is accompanied by a significant decrease in terms of indoor air temperature met ratio during both summer and winter (as reported in Table 5); in addition, a worst relevance of deviations from desired indoor air temperature is also recognized during both heating and cooling seasons (as indicated in Table 5);
- fault 8 increases the total daily electrical energy consumption, operating costs as well as global equivalent CO_2 emissions of the humidifier, the refrigeration system (together with its circulating pump) and the heat pump (together with its circulating pump) with differences equal to about 63%÷64% during summer and around 82%÷85% during winter. During both summer and winter faulty tests, the RS (together with its circulating pump PRS) and the humidifier significantly increase (by at least 20.0% during summer and 7.5% during winter) their operating time to compensate the effects of this fault (as reported in Tables 11 and A.6);
- fault 10 obviously reduces by more than about 77% the daily electrical energy consumption, operational costs, and global equivalent CO_2 emissions of the return air fan itself during both summer and winter. In addition, during the winter faulty test WF10 the humidifier is characterized by a relevant increase in terms of E_{el}, OC and mCO_2 by around 732%, 665% and 625%, respectively, due to that fact that the occurrence of this fault increases the outside air flowrate characterized by lower humidity ratio in comparison to the return air, thus requiring a longer operation of the humidifier (as indicated in Tables 11 and A.6). The differences between faulty and normal tests in terms of total daily energy consumption, operation costs, and global equivalent CO_2 emissions are almost limited and equal to –3% during summer and 8% during winter. In addition, air quality inside the test room is probably affected due to reduced volume air changes;
- fault 11 has a significant impact on the daily electrical energy consumption, operation costs, and global equivalent CO_2 emissions of the heat pump, the refrigeration system and the supply air fan, with reductions equal to about –98%, –44% and –73%, respectively, during summer and around –20%÷–25%, –29% and –75%,

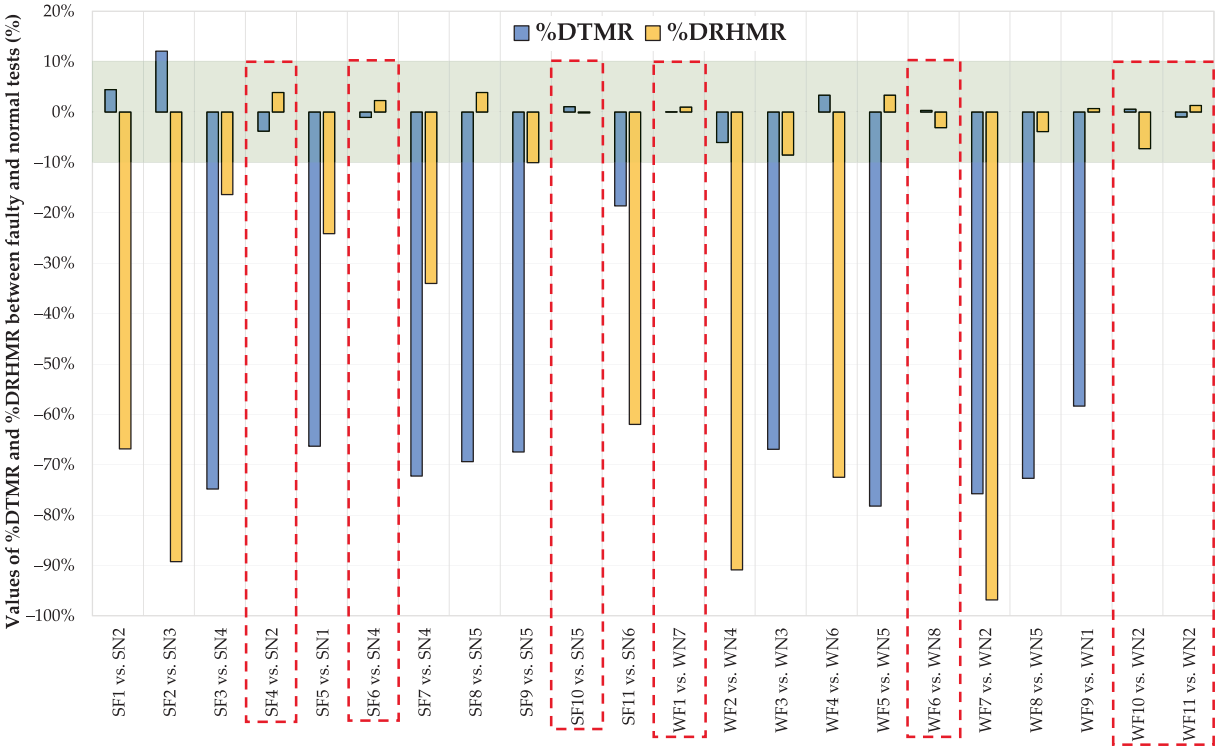


Fig. 6. Percentage difference between faulty and normal tests in terms of time percentage during which indoor air temperature/relative humidity is within the desired deadbands during summer and winter.

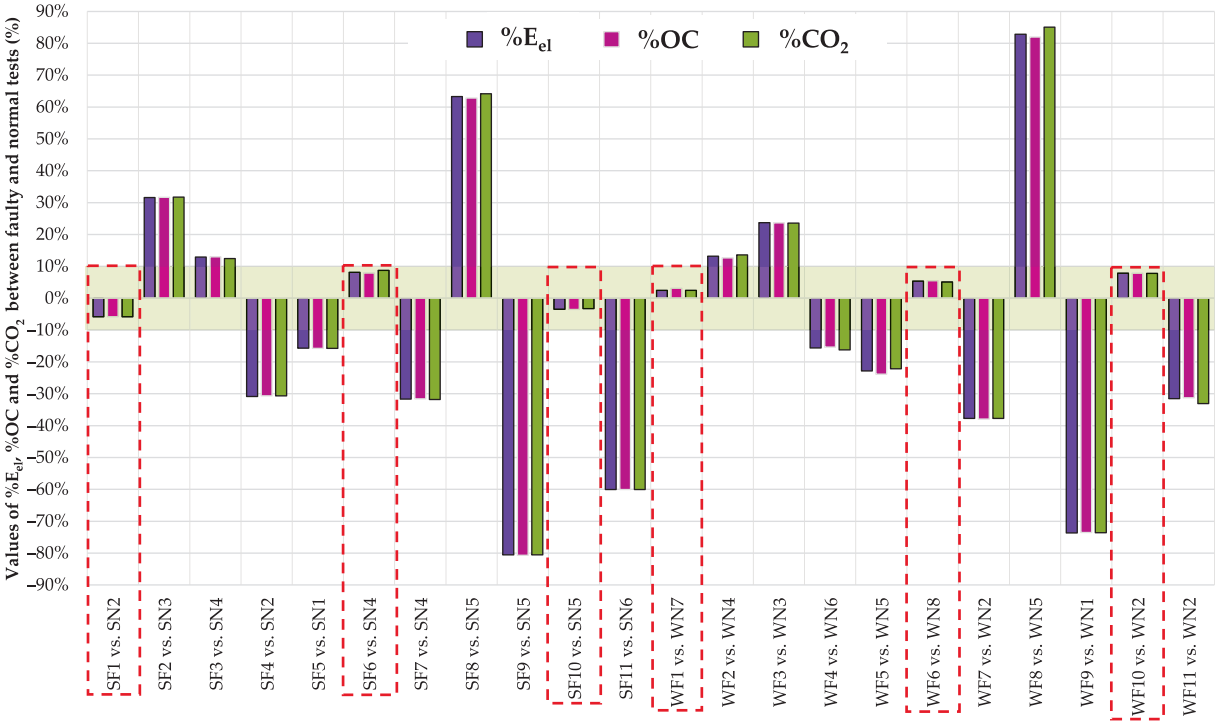


Fig. 7. Percentage difference between faulty and normal tests in terms of daily electrical energy consumption, operating costs and global equivalent CO_2 emissions during summer and winter.

respectively, during winter. The differences between faulty and normal tests in terms of total E_{el}, OC and mCO_2 are equal to around –60% during summer and about –31%÷–33% during winter. However, these decreases are counterbalanced during summer with an important reduction of both indoor air temperature and relative humidity met ratios (as reported in Table 5). In addition, it should be highlighted that the complete failure of the supply air fan will surely affect/reduce the volume air change and, therefore, the indoor air quality.

The faults with the highest (greater than 20%) increases in terms of total daily electricity consumption are the fault 8 during both summer and winter, the fault 2 during summer, and the fault 3 during winter. Fault 8 results in higher total daily electricity demand in summer (63.3%) and winter (82.8%) because the heating coil supply valve is always open (stuck at 100%), causing the heat pump to work much harder; this also means that the cooling coil has to operate longer to balance out the prolonged activation of the heating coil battery and control the temperature of return air; the increased operation of the cooling coil also leads to greater dehumidification of return air and, therefore, also causes a more intensive use of the humidifier. The fault 2 during summer causes a larger total daily electricity consumption due to the fact that the relative humidity sensor reading of return air is incorrect (the read value is always 15% lower than the actual value), which mainly results in a much more significant energy electric demand of the humidifier. A much higher total daily electricity consumption is also found in the case of the fault 3 during winter, as the reading of the sensor measuring return air temperature is always 3 °C lower than the actual temperature; this leads to a greater electricity request by both the heat pump (to increase the return air temperature) and by the humidifier (to enhance the return air relative humidity), thus compensating for the effects of the fault.

Similar considerations underlie the worst values found in terms of operating costs and global equivalent CO_2 emissions.

5.8. Comparative analysis of faults' severity

Fig. 6 summarizes the intensity of the effects related to each analysed fault in terms of indoor air temperature and relative humidity met ratios by reporting, respectively, the percentage differences %DTMR and %DRHMR between corresponding faulty and normal tests:

$$\%DTMR = TMR_{Faulty} - TMR_{Baseline} \quad (37)$$

$$\%DRHMR = RHMR_{Faulty} - RHMR_{Baseline} \quad (38)$$

where TMR_{Faulty} and $TMR_{Baseline}$, respectively, are the percentages of time during which indoor air temperature is maintained within the specified deadbands during the faulty test and its corresponding normal test, while $RHMR_{Faulty}$ and $RHMR_{Baseline}$, respectively, are the percentages of time during which indoor air relative humidity is maintained within the desired upper and lower deadbands of $RH_{SP,Room}$ during the faulty test and its corresponding normal test. The dashed red rectangles in this figure are reported in the cases of the fault is not really effective (i.e., %DTMR and %DRHMR both within ± 10%).

On the other hand, Fig. 7 reports the impact intensity of the analysed faults in terms of total daily electrical energy consumption, operational costs and global equivalent CO_2 emissions. The dashed red rectangles in this figure are reported for the tests where the occurrence of faulty condition is not relevant (i.e., within ± 10%).

Specifically, from Fig. 6 it can be derived that the following faults do not significantly affect indoor thermo-hygrometric met ratios:

- humidifier valve always kept fully closed during the summer faulty tests SF4;
- the cooling coil valve always kept fully open during the summer faulty test SF6;
- the complete failure of the return air fan implemented during the summer faulty test SF10;
- the positive offset of the return air relative humidity sensor kept equal to + 15% artificially introduced during the winter faulty test WF1;
- the cooling coil valve always kept fully open during the winter faulty test WF6;
- the complete failure of the return air fan implemented during the winter faulty test WF10;
- the complete failure of the supply air fan introduced during the winter faulty test WF11.

On the opposite, all the other faults have a clear impact on at least one of the two indoor considered met ratios.

Similarly, Fig. 7 shows that the following list of faults are characterized by a marginal impact in terms of total daily electrical energy consumption, operational costs, as well as global equivalent CO_2 emissions:

- the positive offset of the return air relative humidity sensor kept equal to + 15%, artificially implemented during the summer faulty test SF1;
- the cooling coil valve always kept fully open during the summer faulty test SF6;

Table 12
Qualitative assessment of fault impact on total daily global equivalent CO_2 emissions, operational costs, electrical energy consumption, indoor air temperature met ratio and relative humidity met ratio.

Faulty and normal tests undercomparison	Daily indoor air temperature met ratio	Daily indoor air relative humidity met ratio	Daily electrical energy consumption	Daily operating costs	Daily global equivalent CO_2 emissions
SF1 vs. SN2	0	– –	0	0	0
SF2 vs. SN3	+	– –	+ +	+ +	+ +
SF3 vs. SN4	– –	–	+	+	+
SF4 vs. SN2	0	0	– –	– –	– –
SF5 vs. SN1	– –	– –	–	–	–
SF6 vs. SN4	0	0	0	0	0
SF7 vs. SN4	– –	– –	– –	– –	– –
SF8 vs. SN5	– –	0	+ +	+ +	+ +
SF9 vs. SN5	– –	–	– –	– –	– –
SF10 vs. SN5	0	0	0	0	0
SF11 vs. SN6	–	– –	– –	– –	– –
WF1 vs. WN7	0	0	0	0	0
WF2 vs. WN4	0	– –	+	+	+
WF3 vs. WN3	– –	0	+ +	+ +	+ +
WF4 vs. WN6	0	– –	–	–	–
WF5 vs. WN5	– –	0	– –	– –	– –
WF6 vs. WN8	0	0	0	0	0
WF7 vs. WN2	– –	– –	– –	– –	– –
WF8 vs. WN5	– –	0	+ +	+ +	+ +
WF9 vs. WN1	– –	0	– –	– –	– –
WF10 vs. WN2	0	0	0	0	0
WF11 vs. WN2	0	0	– –	– –	– –

- the complete failure of the winter return air fan implemented during the faulty test SF10;
- the positive offset of the return air relative humidity sensor kept equal to + 15%, introduced during the winter faulty test WF1;
- the cooling coil valve always kept fully open during the winter faulty test WF6;
- the complete failure of the return air fan implemented during the winter faulty test WF10.

For the sake of completeness, the impact intensity of each fault is indicated in Table 12 by using the following qualitative scale conceived to enhance the readability of the results obtained:

- "0″ means that the fault causes not substantial changes (differences within ± 10%);
- "+" means that the fault causes slightly positive changes (differences between 10 and 20%);
- "+ +" means that the fault causes substantial positive changes (differences higher than 20%);
- "–" means that the fault causes slightly negative changes (differences between –10 and –20%);
- "– –" means that the fault causes substantial negative changes (differences lower than –20%).

According to Table 12, the most impactful fault, i.e. that one marked with this symbol "+ +" or this symbol "– –" with reference to all the selected five parameters (i.e., daily indoor air temperature met ratio, daily indoor air relative humidity met ratio, total electrical energy consumption, global equivalent CO_2 emissions and operational costs) is the post-heating coil valve remained closed (stuck at 0%) during both summer and winter. Then, the faults marked with the symbol "+ +" or the symbol "– –" with reference to four out of the selected five parameters are the following ones: negative offset equal to –15% of the return air relative humidity sensor during summer, post-heating coil valve fully open (stuck at 100%) during summer and winter, cooling coil valve fully closed (stuck at 0%) during both summer and winter, complete failure of the supply air fan during summer, negative offset equal to –3.0 °C of the return air temperature sensor readings during winter, and positive offset equal to + 3.0 °C of the return air temperature sensor readings during winter.

6. Conclusions

The study evaluated the impact of 11 common faults on indoor thermal and hygrometric conditions, electrical power demand, electric energy consumption, operational costs as well as global equivalent CO_2 emissions of components in a typical Air-Handling Unit; this assessment was based on the comparison of experimental data from normal and faulty tests conducted during summer and winter in southern Italy, under similar conditions.

The results highlighted that the post-heating coil valve always kept fully open, the negative offset of the return air relative humidity sensor kept constant and equal to –15%, and the negative offset equal to –3.0 °C of the return air temperature sensor have the most adverse effects on daily total electrical energy consumption, operational costs, as well as of global equivalent CO_2 emissions during both summer and winter tests. In terms of indoor air relative humidity met ratio, the negative offset of the return air relative humidity sensor kept constant and equal to –15% as well as the post–heating coil valve always kept closed were the most detrimental ones during both seasons. The faults that negatively impacted indoor air temperature met ratio the most were the negative offset (–3.0 °C) of the return air temperature sensor, the positive offset (+3.0 °C) of the return air temperature sensor, the post-heating coil valve always kept closed, the post-heating coil valve always kept fully open as well as the cooling coil valve always kept closed.

The compiled database will be publicly available for research and institutional use by various entities, including research organizations, AFDD users, and developers. This study generated detailed experimental data that can support advances in both fault diagnosis and system optimization; the field data also provide a useful basis for ranking faults and performing a more accurate cost-benefit analysis of maintenance strategies.

As a next step, the authors aim to expand the database by considering different fault types, including scenarios involving multiple simultaneous faults, diverse fault severities, and a broader range of operating conditions. This will allow to experimentally identify critical thresholds (e.g., fault severity levels) where the energy, environmental and economic impacts escalate sharply. Additionally, they will develop a detailed dynamic simulation model of the AHU, verified against normal and faulty experimental data, to explore a wider set of faulty scenarios under varied operational contexts. In addition, in the future the authors would like to investigate how AHU faults affect long-term economic costs beyond direct energy expenses. With reference to this aspect, it should be underlined that persistent AHU failures can cause abnormal operation, accelerating wear on AHU components and increasing maintenance frequency and, therefore, raising replacement costs. In buildings where thermal comfort or air quality is critical, these faults may also lead to productivity losses or non-compliance with regulatory standards, with potential financial implications. Moreover, unresolved faults can escalate into major failures, turning what could be minor operational expenses into additional and significant capital costs. Although a quantitative analysis of these aspects falls outside the scope of this work, we agree that they are crucial to consider when assessing the overall relevance of fault impact analysis and detection strategies. To better capture the full environmental relevance of AHU faults and overcome some limitations of the current study, future research will include Life Cycle Assessment approaches that account for both operational and embodied emissions related to specific faults. A final objective will be then to create and validate a data-driven algorithm that make use of experimental results for robustly deploy AFDD analyses to be easily scaled on typical AHUs.

CRediT authorship contribution statement

Antonio Rosato: Writing – review & editing, Writing – original draft, Visualization, Validation, Supervision, Software, Resources, Project administration, Methodology, Investigation, Funding acquisition, Formal analysis, Data curation, Conceptualization. **Mohammad El Youssef:** Writing – review & editing, Writing – original draft, Visualization, Validation, Software, Methodology, Investigation, Formal analysis, Data curation. **Rita Mercuri:** Writing – review & editing, Writing – original draft, Visualization, Validation, Software, Methodology, Investigation, Formal analysis, Data curation. **Marco Savino Piscitelli:** Writing – review & editing, Writing – original draft, Visualization, Validation, Supervision, Software, Methodology, Investigation, Formal analysis, Data curation, Conceptualization. **Alfonso Capozzoli:** Writing – review & editing, Writing – original draft, Visualization, Validation, Supervision, Software, Resources, Project administration, Methodology, Investigation, Funding acquisition, Formal analysis, Data curation, Conceptualization.

Declaration of competing interest

The authors declare that they have no known competing financial interests or personal relationships that could have appeared to influence the work reported in this paper.

Acknowledgments

This study has been performed within the activities of the research project titled "UTMOST FDD: an aUToMated, Open, Scalable and Transparent Fault Detection and Diagnosis process for air-handling units

based on a hybrid expert and artificial intelligence approach. From experimental open data to transfer model learning for the enhancement of energy management and indoor environmental quality in buildings" funded by the call "PRIN 22" (CUP: E53D23002840006).

Appendix A

Table A.1 reports the values of dT_{max}, dT_{tot}, dRH_{max}, and dRH_{tot} (defined by Eqs. 24–27) upon varying the normal/faulty test.

Table A.1
Values of dT_{max}, dT_{tot}, dRH_{max}, and dRH_{tot} upon varying the normal/faulty test.

	dT_{max} (° C)	dT_{tot} (° C)	dRH_{max} (%)	dRH_{tot} (%)
SN2	1.3	3318.7	6.3	4551.2
SF1	1.1	1023.2	4.9	53182.3
SN3	1.1	2865.3	6.9	8211.8
SF2	1.2	1371.9	20.7	381609.1
SN4	1.1	2486.7	7.0	5269.6
SF3	3.3	69292.1	6.0	14489.9
SN2	1.3	3318.7	6.3	4551.2
SF4	1.2	2313.6	5.5	1409.9
SN1	1.1	3033.7	12.6	18152.1
SF5	3.1	58986.3	7.1	31561.6
SN4	1.1	2486.7	7.0	5269.6
SF6	1.4	1933.8	4.3	1355.1
SN4	1.1	2486.7	7.0	5269.6
SF7	5.5	121334.1	6.9	34473.3
SN5	1.3	3214.9	8.0	13759.9
SF8	3.3	80458.4	5.2	2768.9
SN5	1.3	3214.9	8.0	13759.9
SF9	3.6	64192.2	9.6	41809.6
SN5	1.3	3214.9	8.0	13759.9
SF10	1.2	2764.6	12.4	15195.7
SN6	1.5	1194.5	8.0	8320.7
SF11	1.2	3112.1	5.8	27395.4
WN7	0.9	1956.9	6.1	2276.4
WF1	1.0	1970.3	6.4	2190.3
WN4	1.0	1325.1	4.8	4200.5
WF2	1.0	4192.4	18.2	281629.5
WN3	1.0	1434.5	5.6	2232.4
WF3	3.4	57910.2	4.9	5115.5
WN6	1.2	3960.0	4.2	2593.6
WF4	1.1	2038.1	6.5	67510.3
WN5	1.3	3717.0	2.5	1576.4
WF5	2.2	53062.6	3.5	974.0
WN8	1.0	2424.3	4.7	3733.6
WF6	1.1	2782.8	7.6	5123.3
WN2	0.9	1336.7	3.5	1259.0
WF7	4.3	98518.6	4.3	93765.9
WN5	1.3	3717.0	2.5	1576.4
WF8	5.9	118150.0	3.8	2562.0
WN1	1.1	1381.1	4.4	1925.0
WF9	1.1	16083.4	5.3	1882.5
WN2	0.9	1336.7	3.5	1259.0
WF10	0.9	2111.5	9.0	8600.3
WN2	0.9	1336.7	3.5	1259.0
WF11	1.0	1238.6	2.5	729.1

Table A.2 reports the values of the μ_{el} and the σ_{el} upon varying both the normal/faulty test as well as the AHU component.

Table A.2
Values of μ_{el} and σ_{el} upon varying both the normal/faulty test as well as the AHU component.

	SAF		RAF		RS		HP		HUM	
	μ_{el} (W)	σ_{el} (W)	μ_{el} (W)	σ_{el} (W)	μ_{el} (W)	σ_{el} (W)	μ_{el} (W)	σ_{el} (W)	μ_{el} (W)	σ_{el} (W)
SN2	337.3	8.3	74.0	1.3	3824.8	1573.9	3659.4	1801.3	3081.2	995.7
SF1	336.1	8.0	73.9	1.3	3781.9	1568.1	3645.6	1790.1	0.0	0.0
SN3	338.5	10.3	73.8	1.9	4479.1	1403.4	4354.2	1657.9	3151.6	936.3
SF2	333.6	13.7	73.7	2.6	5139.0	429.5	5351.8	508.3	3461.2	484.4
SN4	341.4	13.8	73.3	2.6	4836.8	547.5	5411.8	560.6	3233.5	885.2
SF3	337.1	14.0	73.2	2.9	4823.3	539.7	5372.0	535.9	3235.3	868.2
SN2	337.3	8.3	74.0	1.3	3824.8	1573.9	3659.4	1801.3	3081.2	995.7

(*continued on next page*)

Table A.2 (*continued*)

	SAF		RAF		RS		HP		HUM	
	μ_{el} (W)	σ_{el} (W)	μ_{el} (W)	σ_{el} (W)	μ_{el} (W)	σ_{el} (W)	μ_{el} (W)	σ_{el} (W)	μ_{el} (W)	σ_{el} (W)
SF4	344.4	14.0	73.6	2.6	4918.7	962.6	5433.5	545.5	0.0	0.0
SN1	343.7	8.4	74.6	3.0	3406.5	1533.2	3571.9	1797.7	3151.5	911.3
SF5	346.4	13.9	73.7	2.6	4812.2	461.3	5442.9	590.0	0.0	0.0
SN4	341.4	13.8	73.3	2.6	4836.8	547.5	5411.8	560.6	3233.5	885.2
SF6	345.1	14.0	73.6	2.5	4824.1	392.5	5359.4	593.6	3281.0	827.4
SN4	341.4	13.8	73.3	2.6	4836.8	547.5	5411.8	560.6	3233.5	885.2
SF7	352.7	13.8	73.8	2.5	4833.9	438.9	0.0	0.0	0.0	0.0
SN5	344.5	14.2	73.7	2.6	4766.5	670.7	5377.8	534.7	3244.7	864.6
SF8	341.2	12.9	73.2	2.6	4821.7	381.6	5376.5	521.0	3425.1	591.0
SN5	344.5	14.2	73.7	2.6	4766.5	670.7	5377.8	534.7	3244.7	864.6
SF9	340.9	13.3	73.1	2.6	4900.7	496.0	0.0	0.0	3075.5	1197.9
SN5	344.5	14.2	73.7	2.6	4766.5	670.7	5377.8	534.7	3244.7	864.6
SF10	333.2	15.8	16.9	0.0	4829.6	444.9	5331.4	551.6	3278.1	830.4
SN6	337.7	13.3	73.5	2.6	4774.3	437.5	5347.3	551.5	0.0	0.0
SF11	92.8	4.4	70.9	3.1	4814.8	474.4	5560.5	461.2	0.0	0.0
WN7	358.6	15.9	75.8	2.8	4691.0	437.1	5955.5	826.2	0.0	0.0
WF1	358.6	15.2	75.6	2.8	4704.9	439.2	6006.9	752.4	0.0	0.0
WN4	346.5	14.2	75.6	2.7	4322.1	384.2	5343.1	762.4	0.0	0.0
WF2	345.6	14.4	74.7	2.7	4277.7	410.3	5356.4	664.6	3263.2	830.3
WN3	350.3	15.0	75.6	4.5	4020.0	388.5	5257.3	876.2	3059.2	1073.5
WF3	346.7	14.1	75.6	2.6	4030.2	354.2	5268.8	832.2	3250.3	845.7
WN6	353.1	14.9	75.6	3.3	4153.7	378.2	5552.0	801.2	3239.6	879.8
WF4	352.8	14.8	75.8	2.7	4160.6	378.6	5549.0	786.9	0.0	0.0
WN5	354.6	15.4	75.9	8.5	4113.7	385.0	5589.8	703.6	3212.2	884.0
WF5	357.5	10.5	76.1	2.7	4141.7	354.6	5620.6	680.1	3040.0	1076.1
WN8	358.6	15.6	75.3	2.7	4636.1	435.7	5965.4	648.0	3143.2	976.4
WF6	357.2	15.4	75.4	2.6	5231.2	485.1	5948.8	887.0	3172.3	939.2
WN2	349.1	16.3	75.6	3.3	4180.4	394.3	5283.8	800.4	2879.5	1374.5
WF7	357.7	13.6	76.3	2.7	4153.6	365.3	5379.7	618.2	0.0	0.0
WN5	354.6	15.4	75.9	8.5	4113.7	385.0	5589.8	703.6	3212.2	884.0
WF8	339.0	13.8	75.4	3.7	4118.8	368.4	5249.3	820.9	3354.0	715.0
WN1	342.7	14.4	75.1	2.7	4080.4	380.5	5265.9	926.6	0.0	0.0
WF9	348.5	3.9	73.3	2.6	4099.2	358.7	5252.9	971.6	0.0	0.0
WN2	349.1	16.3	75.6	3.3	4180.4	394.3	5283.8	800.4	2879.5	1374.5
WF10	341.0	16.8	16.9	0.1	4176.0	354.6	5283.4	848.8	3236.3	886.2
WN2	349.1	16.3	75.6	3.3	4180.4	394.3	5283.8	800.4	2879.5	1374.5
WF11	87.9	1.6	73.4	3.6	4219.7	389.9	5360.7	628.9	0.0	0.0

Table A.3 reports the values of E_{el} upon varying both the normal/faulty test as well as the AHU component.

Table A.3
Values of E_{el} upon varying both the normal/faulty test as well as the AHU component during the summer and winter.

	SAF	RAF	RS + PRS	HP + PHP	HUM	TOTAL
E_{el} of SN2 (kWh)	3.0	0.7	28.5	9.3	5.1	46.6
E_{el} of SF1 (kWh)	3.0	0.7	29.6	10.5	0.0	43.8
E_{el} of SN3 (kWh)	3.0	0.7	28.5	10.3	4.4	46.9
E_{el} of SF2 (kWh)	3.0	0.7	29.7	3.2	25.2	61.8
E_{el} of SN4 (kWh)	3.1	0.7	26.0	10.1	4.3	44.1
E_{el} of SF3 (kWh)	3.0	0.7	22.6	13.2	10.3	49.8
E_{el} of SN2 (kWh)	3.0	0.7	28.5	9.3	5.1	46.6
E_{el} of SF4 (kWh)	3.1	0.7	20.5	7.9	0.0	32.2
E_{el} of SN1 (kWh)	3.1	0.7	22.4	9.6	5.3	41.0
E_{el} of SF5 (kWh)	3.1	0.7	25.9	4.9	0.0	34.6
E_{el} of SN4 (kWh)	3.1	0.7	26.0	10.1	4.3	44.1
E_{el} of SF6 (kWh)	3.1	0.7	28.6	9.4	6.0	47.7
E_{el} of SN4 (kWh)	3.1	0.7	26.0	10.1	4.3	44.1
E_{el} of SF7 (kWh)	3.2	0.7	26.3	0.0	0.0	30.2
E_{el} of SN5 (kWh)	3.1	0.7	23.7	8.6	5.7	41.8
E_{el} of SF8 (kWh)	3.1	0.7	28.8	16.0	19.6	68.2
E_{el} of SN5 (kWh)	3.1	0.7	23.7	8.6	5.7	41.8
E_{el} of SF9 (kWh)	3.1	0.7	3.8	0.0	0.6	8.1
E_{el} of SN5 (kWh)	3.1	0.7	23.7	8.6	5.7	41.8
E_{el} of SF10 (kWh)	3.0	0.2	22.1	9.6	5.5	40.3
E_{el} of SN6 (kWh)	3.0	0.7	24.8	10.6	0.0	39.0
E_{el} of SF11 (kWh)	0.8	0.6	13.9	0.2	0.0	15.6
E_{el} of WN7 (kWh)	3.2	0.7	15.4	12.8	0.0	32.2
E_{el} of WF1 (kWh)	3.2	0.7	15.7	13.4	0.0	33.0
E_{el} of WN4 (kWh)	3.1	0.7	16.0	10.9	0.0	30.7
E_{el} of WF2 (kWh)	3.1	0.7	14.8	7.4	8.9	34.8

(*continued on next page*)

Table A.3 (*continued*)

	SAF	RAF	RS + PRS	HP + PHP	HUM	TOTAL
E_{el} of WN3 (kWh)	3.2	0.7	13.0	12.5	1.6	31.0
E_{el} of WF3 (kWh)	3.1	0.7	11.7	17.7	5.1	38.3
E_{el} of WN6 (kWh)	3.2	0.7	13.1	6.9	4.1	28.0
E_{el} of WF4 (kWh)	3.2	0.7	13.0	6.7	0.0	23.6
E_{el} of WN5 (kWh)	3.2	0.7	13.3	7.2	3.5	27.9
E_{el} of WF5 (kWh)	3.2	0.7	14.6	1.4	1.6	21.5
E_{el} of WN8 (kWh)	3.2	0.7	15.1	14.2	2.7	35.9
E_{el} of WF6 (kWh)	3.2	0.7	15.2	15.1	3.6	37.8
E_{el} of WN2 (kWh)	3.1	0.7	14.4	10.0	0.4	28.7
E_{el} of WF7 (kWh)	3.2	0.7	13.4	0.6	0.0	17.9
E_{el} of WN5 (kWh)	3.2	0.7	13.3	7.2	3.5	27.9
E_{el} of WF8 (kWh)	3.1	0.7	15.5	21.3	10.5	51.0
E_{el} of WN1 (kWh)	3.1	0.7	12.9	13.6	0.0	30.2
E_{el} of WF9 (kWh)	3.1	0.7	1.5	2.6	0.0	8.0
E_{el} of WN2 (kWh)	3.1	0.7	14.4	10.0	0.4	28.7
E_{el} of WF10 (kWh)	3.1	0.2	11.9	12.3	3.5	30.9
E_{el} of WN2 (kWh)	3.1	0.7	14.4	10.0	0.4	28.7
E_{el} of WF11 (kWh)	0.8	0.7	10.2	8.0	0.0	19.6

Table A.4 reports the values of OC upon varying both the normal/faulty test as well as the AHU component.

Table A.4
Values of OC upon varying both the normal/faulty test as well as the AHU component.

	SAF	RAF	RS + PRS	HP + PHP	HUM	TOTAL
OC of SN2 (€)	0.3	0.1	3.0	1.0	0.5	4.9
OC of SF1 (€)	0.3	0.1	3.1	1.1	0.0	4.6
OC of SN3 (€)	0.4	0.1	3.3	1.2	0.5	5.5
OC of SF2 (€)	0.4	0.1	3.5	0.4	3.0	7.2
OC of SN4 (€)	0.4	0.1	3.0	1.2	0.5	5.0
OC of SF3 (€)	0.3	0.1	2.6	1.5	1.2	5.7
OC of SN2 (€)	0.4	0.1	3.4	1.1	0.6	5.6
OC of SF4 (€)	0.4	0.1	2.5	1.0	0.0	3.9
OC of SN1 (€)	0.3	0.1	2.4	1.0	0.6	4.5
OC of SF5 (€)	0.3	0.1	2.8	0.5	0.0	3.8
OC of SN4 (€)	0.3	0.1	2.8	1.1	0.5	4.8
OC of SF6 (€)	0.3	0.1	3.1	1.0	0.6	5.2
OC of SN4 (€)	0.4	0.1	3.4	1.3	0.6	5.8
OC of SF7 (€)	0.4	0.1	3.5	0.0	0.0	4.0
OC of SN5 (€)	0.4	0.1	3.1	1.1	0.8	5.5
OC of SF8 (€)	0.4	0.1	3.8	2.1	2.6	9.0
OC of SN5 (€)	0.4	0.1	3.1	1.1	0.7	5.4
OC of SF9 (€)	0.4	0.1	0.5	0.0	0.1	1.0
OC of SN5 (€)	0.4	0.1	3.3	1.2	0.8	5.8
OC of SF10 (€)	0.4	0.0	3.0	1.3	0.8	5.6
OC of SN6 (€)	0.4	0.1	3.5	1.5	0.0	5.4
OC of SF11 (€)	0.1	0.1	1.9	0.0	0.0	2.2
OC of WN7 (€)	0.8	0.2	3.6	3.2	0.0	7.7
OC of WF1 (€)	0.8	0.2	3.7	3.3	0.0	8.0
OC of WN4 (€)	0.8	0.2	3.9	2.7	0.0	7.5
OC of WF2 (€)	0.8	0.2	3.6	1.8	2.1	8.4
OC of WN3 (€)	1.5	0.3	6.1	6.0	0.8	14.7
OC of WF3 (€)	1.5	0.3	5.5	8.4	2.4	18.2
OC of WN6 (€)	0.7	0.2	2.9	1.6	0.9	6.2
OC of WF4 (€)	0.7	0.2	2.9	1.5	0.0	5.3
OC of WN5 (€)	0.7	0.2	3.0	1.7	0.8	6.3
OC of WF5 (€)	0.7	0.2	3.3	0.3	0.3	4.8
OC of WN8 (€)	1.5	0.3	6.8	6.5	1.2	16.3
OC of WF6 (€)	1.5	0.3	6.9	7.0	1.6	17.2
OC of WN2 (€)	1.2	0.3	5.7	3.9	0.2	11.3
OC of WF7 (€)	1.3	0.3	5.3	0.2	0.0	7.0
OC of WN5 (€)	1.0	0.2	4.3	2.4	1.1	9.1
OC of WF8 (€)	1.0	0.2	5.1	7.0	3.4	16.6
OC of WN1 (€)	0.8	0.2	3.2	3.4	0.0	7.5
OC of WF9 (€)	0.8	0.2	0.4	0.7	0.0	2.0
OC of WN2 (€)	1.3	0.3	5.8	4.0	0.2	11.5
OC of WF10 (€)	1.2	0.1	4.7	4.9	1.4	12.4
OC of WN2 (€)	1.2	0.3	5.3	3.7	0.2	10.6
OC of WF11 (€)	0.3	0.2	3.8	3.0	0.0	7.3

Table A.5 reports the values of mCO_2 upon varying both the normal/faulty test as well as the AHU component.

Table A.5
Values of mCO_2 upon varying both the normal/faulty test as well as the AHU component.

	SAF	RAF	RS + PRS	HP + PHP	HUM	TOTAL
mCO_2 of SN2 (gCO_2)	878.3	192.6	8235.3	2700.7	1454.7	13461.7
mCO_2 of SF1 (gCO_2)	874.8	192.4	8540.7	3064.6	0.0	12672.6
mCO_2 of SN3 (gCO_2)	1121.1	244.4	10484.5	3767.7	1647.4	17265.1
mCO_2 of SF2 (gCO_2)	1103.5	243.9	10923.5	1178.1	9296.6	22745.5
mCO_2 of SN4 (gCO_2)	941.2	201.8	7977.6	3094.6	1312.7	13527.9
mCO_2 of SF3 (gCO_2)	929.5	201.8	6892.9	4050.6	3139.4	15214.3
mCO_2 of SN2 (gCO_2)	951.8	208.7	8919.0	2910.1	1579.2	14568.9
mCO_2 of SF4 (gCO_2)	972.1	207.8	6435.5	2487.9	0.0	10103.2
mCO_2 of SN1 (gCO_2)	660.7	143.4	4777.8	2068.4	1174.3	8824.6
mCO_2 of SF5 (gCO_2)	666.2	141.8	5528.5	1096.2	0.0	7432.7
mCO_2 of SN4 (gCO_2)	955.4	204.9	8114.6	3131.5	1334.7	13741.1
mCO_2 of SF6 (gCO_2)	964.9	206.0	8905.4	2936.2	1929.3	14941.7
mCO_2 of SN4 (gCO_2)	978.5	209.9	8296.1	3214.6	1356.9	14056.0
mCO_2 of SF7 (gCO_2)	1009.8	211.5	8362.4	0.0	0.0	9583.7
mCO_2 of SN5 (gCO_2)	844.5	180.7	6472.5	2348.8	1554.5	11401.1
mCO_2 of SF8 (gCO_2)	835.7	179.3	7891.7	4356.6	5452.8	18716.0
mCO_2 of SN5 (gCO_2)	787.4	168.5	6030.1	2189.8	1450.1	10625.9
mCO_2 of SF9 (gCO_2)	778.5	166.8	962.4	0.0	156.1	2063.8
mCO_2 of SN5 (gCO_2)	1021.3	218.6	7825.2	2837.6	1876.8	13779.5
mCO_2 of SF10 (gCO_2)	987.9	50.1	7353.3	3198.3	1740.9	13330.5
mCO_2 of SN6 (gCO_2)	1053.0	229.3	8597.9	3652.4	0.0	13532.6
mCO_2 of SF11 (gCO_2)	290.4	221.0	4836.4	59.2	0.0	5407.1
mCO_2 of WN7 (gCO_2)	1245.0	263.1	5945.0	4936.2	0.0	12389.3
mCO_2 of WF1 (gCO_2)	1244.9	262.5	6045.5	5140.9	0.0	12693.8
mCO_2 of WN4 (gCO_2)	1066.1	232.5	5476.7	3657.1	0.0	10432.5
mCO_2 of WF2 (gCO_2)	1063.6	229.9	5052.3	2510.2	2993.3	11849.2
mCO_2 of WN3 (gCO_2)	1365.2	294.7	5615.8	5395.9	728.8	13400.3
mCO_2 of WF3 (gCO_2)	1351.6	294.7	5052.1	7610.1	2249.2	16557.8
mCO_2 of WN6 (gCO_2)	1180.1	252.6	4835.2	2547.8	1544.6	10360.4
mCO_2 of WF4 (gCO_2)	1179.0	253.2	4806.4	2439.4	0.0	8678.0
mCO_2 of WN5 (gCO_2)	1029.9	220.4	4260.0	2341.0	1150.3	9001.6
mCO_2 of WF5 (gCO_2)	1037.7	220.8	4722.9	469.9	558.9	7010.2
mCO_2 of WN8 (gCO_2)	1160.4	243.7	5425.7	5122.9	978.4	12931.2
mCO_2 of WF6 (gCO_2)	1155.8	243.9	5437.0	5462.9	1289.2	13588.7
mCO_2 of WN2 (gCO_2)	1094.6	237.2	5023.0	3473.5	150.8	9979.1
mCO_2 of WF7 (gCO_2)	1121.4	239.1	4659.3	193.8	0.0	6213.6
mCO_2 of WN5 (gCO_2)	907.6	194.2	3763.1	2038.8	1018.8	7922.4
mCO_2 of WF8 (gCO_2)	866.6	192.8	4430.5	6049.9	3122.1	14661.9
mCO_2 of WN1 (gCO_2)	939.6	205.8	3912.3	4161.3	0.0	9219.0
mCO_2 of WF9 (gCO_2)	955.4	200.9	470.8	809.4	0.0	2436.6
mCO_2 of WN2 (gCO_2)	957.0	207.4	4372.6	3058.2	147.4	8742.5
mCO_2 of WF10 (gCO_2)	935.0	46.4	3605.1	3767.2	1068.3	9422.1
mCO_2 of WN2 (gCO_2)	992.1	215.0	4541.3	3156.6	152.0	9057.1
mCO_2 of WF11 (gCO_2)	249.6	208.6	3221.5	2383.3	0.0	6063.0

Table A.6 reports values of OT upon varying both the normal/faulty test as well as the AHU component.

Table A.6
Values of OT upon varying both the normal/faulty test as well as the AHU component.

	SAF	RAF	RS	HP	HUM	PRS	PHP
OT of SN2 (min)	540.0	540.0	345.3	83.1	98.7	484.2	319.2
OT of SF1 (min)	540.0	540.0	355.4	97.9	0.0	540.0	347.2
OT of SN3 (min)	539.5	539.8	299.3	76.6	83.9	465.7	363.1
OT of SF2 (min)	538.7	539.5	274.4	17.6	436.8	464.9	126.6
OT of SN4 (min)	538.7	539.6	241.9	64.2	79.2	488.4	330.2
OT of SF3 (min)	538.5	539.4	220.4	80.5	190.2	371.4	460.1
OT of SN2 (min)	540.0	540.0	345.3	83.1	98.7	484.2	319.2
OT of SF4 (min)	538.8	539.6	197.6	45.7	0.0	325.9	285.4
OT of SN1 (min)	540.0	539.4	293.1	89.0	101.6	433.2	324.2
OT of SF5 (min)	538.7	539.6	234.3	32.2	0.0	538.7	148.6
OT of SN4 (min)	538.7	539.6	241.9	64.2	79.2	488.4	330.2
OT of SF6 (min)	538.7	539.5	266.8	60.3	109.5	540.0	302.5
OT of SN4 (min)	538.7	539.6	241.9	64.2	79.2	488.4	330.2
OT of SF7 (min)	538.7	539.6	238.3	0.0	0.0	538.4	0.0
OT of SN5 (min)	538.7	539.5	224.9	54.1	105.2	440.8	285.1
OT of SF8 (min)	538.7	539.6	269.9	99.3	343.0	538.7	540.0
OT of SN5 (min)	538.7	539.5	224.9	54.1	105.2	440.8	285.1
OT of SF9 (min)	538.7	539.6	46.1	0.0	12.5	0.0	0.0
OT of SN5 (min)	538.7	539.5	224.9	54.1	105.2	440.8	285.1

(*continued on next page*)

Table A.6 (*continued*)

	SAF	RAF	RS	HP	HUM	PRS	PHP
OT of SF10 (min)	538.7	0.0	200.8	60.2	100.4	448.1	322.2
OT of SN6 (min)	538.7	539.6	221.5	70.2	0.0	538.5	327.9
OT of SF11 (min)	0.2	539.6	84.3	2.0	0.0	538.7	0.0
OT of WN7 (min)	538.7	539.5	106.1	99.9	0.0	538.3	221.5
OT of WF1 (min)	538.7	539.5	109.2	103.2	0.0	538.4	231.5
OT of WN4 (min)	538.7	539.5	123.5	82.9	0.0	538.7	266.7
OT of WF2 (min)	538.7	539.5	126.3	54.3	163.0	436.9	191.5
OT of WN3 (min)	538.7	539.5	86.6	103.4	32.3	538.2	267.3
OT of WF3 (min)	538.7	539.5	86.1	140.6	94.8	443.6	409.3
OT of WN6 (min)	538.7	539.5	96.2	56.3	75.8	482.5	130.6
OT of WF4 (min)	538.7	539.5	97.6	54.5	0.0	469.8	127.0
OT of WN5 (min)	538.7	539.5	96.7	62.5	65.8	501.3	107.9
OT of WF5 (min)	539.3	539.5	108.2	15.4	31.7	538.3	0.0
OT of WN8 (min)	538.6	539.5	103.5	110.1	51.3	535.7	244.6
OT of WF6 (min)	538.7	539.5	92.4	118.4	68.0	538.6	256.2
OT of WN2 (min)	538.7	539.5	104.6	79.5	8.8	538.8	226.6
OT of WF7 (min)	538.7	539.5	90.2	6.2	0.0	538.3	0.0
OT of WN5 (min)	538.7	539.5	96.7	62.5	65.8	501.3	107.9
OT of WF8 (min)	538.7	539.5	122.2	163.3	187.1	538.8	540.0
OT of WN1 (min)	538.7	539.5	84.1	111.1	0.0	538.6	294.1
OT of WF9 (min)	540.0	539.5	22.7	26.2	0.0	0.0	25.2
OT of WN2 (min)	538.7	539.5	104.6	79.5	8.8	538.8	226.6
OT of WF10 (min)	538.7	0.0	74.0	96.2	65.4	508.6	289.3
OT of WN2 (min)	538.7	539.5	104.6	79.5	8.8	538.8	226.6
OT of WF11 (min)	0.0	539.3	43.4	36.4	0.0	538.4	359.8

Data availability

Data will be made available on request.

References

[1] Global Alliance for Buildings and Construction, Global status report for buildings and construction 2024/2025. https://globalabc.org/sites/default/files/2025-03/Global-Status-Report-2024_2025.pdf, 2025 (accessed 14 July 2025).

[2] X. Cao, X. Dai, J. Liu, Building energy-consumption status worldwide and the state-of-the-art technologies for zero-energy buildings during the past decade, Energy Build. 128 (2016) 198–213, https://doi.org/10.1016/j.enbuild.2016.06.089.

[3] W.S. Yun, W.H. Hong, H. Seo, A data-driven fault detection and diagnosis scheme for air handling units in building HVAC systems considering undefined states, J. Build. Eng. 35 (2021) 102056, https://doi.org/10.1016/j.jobe.2020.102056.

[4] M.S. Mirnaghi, F. Haghighat, Fault detection and diagnosis of large-scale HVAC systems in buildings using data-driven methods: a comprehensive review, Energy Build. 229 (2020) 110492, https://doi.org/10.1016/j.enbuild.2020.110492.

[5] Council of the European Union, Council adopts Energy Efficiency Directive, 25 July 2023. https://www.consilium.europa.eu/en/press/press-releases/2023/07/25/council-adopts-energy-efficiency-directive/, 2023 (accessed 14 July 2025).

[6] J. Proctor, Residential and small commercial central air conditioning; rated efficiency isn't automatic. Proceedings of the ASHRAE Winter Meeting, Anaheim, CA, USA, 2004.

[7] T.M. Rossi, Unitary air conditioner field performance. Proceedings of the International Refrigeration and Air Conditioning Conference, Purdue University, West Lafayette, IN, USA, 2004.

[8] J. Schein, S.T. Bushby, N.S. Castro, J.M. House, A rule-based fault detection method for air handling units, Energy Build. 38 (12) (2006) 1485–1492, https://doi.org/10.1016/j.enbuild.2006.03.017.

[9] S. Katipamula, M.R. Brambley, Methods for fault detection, diagnostics, and prognostics for building systems – a review, part II, HVAC&R Res. 11 (2) (2005) 169–187, https://doi.org/10.1080/10789669.2005.10391138.

[10] S. Wu, J.Q. Sun, Cross-level fault detection and diagnosis of building HVAC systems, Build. Environ. 46 (8) (2011) 1558–1566, https://doi.org/10.1016/j.buildenv.2011.01.027.

[11] H. Wang, Y. Chen, A robust fault detection and diagnosis strategy for multiple faults of VAV air handling units, Energy Build. 127 (2016) 442–451, https://doi.org/10.1016/j.enbuild.2016.06.016.

[12] G. Lin, H. Kramer, J. Granderson, Building fault detection and diagnostics: Achieved savings, and methods to evaluate algorithm performance, Build. Environ. 168 (2020) 106505, https://doi.org/10.1016/j.buildenv.2019.106505.

[13] Y. Zhao, T. Li, X. Zhang, C. Zhang, Artificial intelligence-based fault detection and diagnosis methods for building energy systems: Advantages, challenges and the future, Renew. Sustain. Energy Rev. 109 (2019) 85–101, https://doi.org/10.1016/j.rser.2019.04.020.

[14] W. Kim, S. Katipamula, A review of fault detection and diagnostics methods for building systems, Sci. Technol. Built Environ. 24 (1) (2018) 3–21, https://doi.org/10.1080/23744731.2017.1314987.

[15] J. Huang, J. Wen, H. Yoon, O. Pradhan, T. Wu, Z. O'Neill, K.S. Candan, Real vs. simulated: questions on the capability of simulated datasets on building fault detection for energy efficiency from a data-driven perspective, Energy Build. 259 (2022) 111872, https://doi.org/10.1016/j.enbuild.2022.111872.

[16] S. Frank, G. Lin, X. Jin, R. Singla, A. Farthing, J. Granderson, A performance evaluation framework for building fault detection and diagnosis algorithms, Energy Build. 192 (2019) 84–92, https://doi.org/10.1016/j.enbuild.2019.03.026.

[17] Y. Yu, D. Woradechjumroen, D. Yu, A review of fault detection and diagnosis methodologies on air-handling units, Energy Build. 82 (2014) 550–562, https://doi.org/10.1016/j.enbuild.2014.07.003.

[18] M.S. Piscitelli, D.M. Mazzarelli, A. Capozzoli, Enhancing operational performance of AHUs through an advanced fault detection and diagnosis process based on temporal association and decision rules, Energy Build. 226 (2020) 110369, https://doi.org/10.1016/j.enbuild.2020.110369.

[19] J. Wen, S. Li, Tools for evaluating fault detection and diagnostic methods for air-handling units, ASHRAE 1312-RP Final Report (2011).

[20] J. Granderson, G. Lin, R. Singla, E. Mayhorn, P. Ehrlich, D. Vrabie, Commercial fault detection and diagnostics tools: What they offer, how they differ, and what's still needed, Lawrence Berkeley National Laboratory Recent Work, 2018, pp. 1–12, https://doi.org/10.20357/B7V88H, 2018 (accessed 27 June 2025).

[21] J. Granderson, G. Lin, A. Harding, P. Im, Y. Chen, Building fault detection data to aid diagnostic algorithm creation and performance testing, Sci. Data 7 (2020) 65, https://doi.org/10.1038/s41597-020-0400-y.

[22] A. Casillas, G. Lin, J. Granderson, Curation of ground-truth validated benchmarking datasets for fault detection & diagnostics tools, Lawrence Berkeley National Laboratory, Berkeley, CA, USA, 2021.

[23] R.I. Hu, J. Granderson, D.M. Auslader, A. Agogino, Design of machine learning models with domain experts for automated sensor selection for energy fault detection, Appl. Energy 235 (2019) 117–128, https://doi.org/10.1016/j.apenergy.2018.10.092.

[24] R. Liu, X. Zhou, R. Milbrandt, Experimental study of lab controlled faults in dual-duct VAV system. Proceedings of the ASHRAE Transactions, Atlanta, GA, USA, 2015.

[25] A. Rosato, F. Guarino, V. Filomena, S. Sibilio, L. Maffei, Experimental calibration and validation of a simulation model for fault detection of HVAC systems and application to a case study, Energies 13 (15) (2020) 3817, https://doi.org/10.3390/en13153817.

[26] A. Rosato, F. Guarino, S. Sibilio, E. Entchev, M. Masullo, L. Maffei, Healthy and faulty experimental performance of a typical HVAC system under Italian climatic conditions: Artificial neural network-based model and fault impact assessment, Energies 14 (171) (2021) 1–24, https://doi.org/10.3390/en14010171.

[27] A. Rosato, F. Guarino, M. El Youssef, S. Sibilio, L. Maffei, Preliminary symptoms assessment of typical faults related to the fans and humidifiers of HVAC systems based on experimental data collected during Italian summer and winter, IOP Conf. Ser.: Earth Environ. Sci 897 (13) (2021) 012013, https://doi.org/10.1088/1755-1315/897/1/012013.

[28] B. Wu, W. Cai, F. Cheng, H. Chen, Simultaneous-fault diagnosis considering time series with a deep learning transformer architecture for air handling units, Energy Build. 257 (2022) 111761, https://doi.org/10.1016/j.enbuild.2021.111761.

[29] H. Liao, W. Cai, F. Cheng, S. Dubey, P.B. Rajesh, An online data-driven fault diagnosis method for air handling units by rule and convolutional neural networks, Sensors 21 (13) (2021) 4391, https://doi.org/10.3390/s21134391.
[30] National Institute of Standards and Technology (NIST), HVAC SIMulation PLUS other systems (HVACSIM+). https://www.nist.gov/services-resources/software/hvac-simulation-plus-other-systems-hvacsim, 2025 (accessed 27 June 2025).
[31] E. Marrasso, C. Martone, G. Pallotta, I. Perugini, C. Roselli, M. Sasso, Environmental impact reduction of residential end-users: an innovative methodology based on the power grid CO_2 emission factor, Energy Build. 348 (2025) 116419, https://doi.org/10.1016/j.enbuild.2025.116419.
[32] X. Lu, Y. Fu, Z. O'Neill, J. Wen, A holistic fault impact analysis of the high-performance sequences of operation for HVAC systems: Modelica-based case study in a medium-office building, Energy Build. 252 (2021) 111448, https://doi.org/10.1016/j.enbuild.2021.111448.
[33] Y. Chen, G. Lin, Z. Chen, J. Wen, J. Granderson, A simulation-based evaluation of fan coil unit fault effects, Energy Build. 263 (2022) 112041, https://doi.org/10.1016/j.enbuild.2022.112041.
[34] Y. Li, Z. O'Neill, A critical review of fault modeling of HVAC systems in buildings, Build. Simul. 11 (5) (2018) 953–975, https://doi.org/10.1007/s12273-018-0469-y.
[35] D. Dey, B. Dong, Z. Li, A probabilistic framework to diagnose faults in air handling units. Proceedings of the International High Performance Buildings Conference, Purdue University, West Lafayette, IN, USA, 2016.
[36] O. Nehasil, L. Dobiášová, V. Mazanec, J. Široký, Versatile AHU fault detection – Design, field validation and practical application, Energy Build. 237 (2021) 110781, https://doi.org/10.1016/j.enbuild.2021.110781.
[37] B. Feng, Q. Zhou, J. Xing, Q. Yang, X. Qin, Y. Mo, W. Chen, A fully distributed voting strategy for AHU fault detection and diagnosis based on a decentralized structure, Energy Rep. 8 (2022) 390–404, https://doi.org/10.1016/j.egyr.2022.01.077.
[38] P. Carling, Comparison of three fault detection and diagnosis methods based on field data of an air handling unit. Proceedings of the ASHRAE Transactions 108, Atlantic City, NJ, USA, 12 January 2002, 2002.
[39] SENS i-Lab, Department of Architecture and Industrial Design, University of Campania Luigi Vanvitelli, 2025. https://www.architettura.unicampania.it/images/ricerca/laboratori/EN/SENS-i_Lab_2025_EN.pdf, 2025 (accessed 14 July 2025).
[40] A. Rosato, F. Guarino, M. El Youssef, A. Capozzoli, M. Masullo, L. Maffei, Faulty operation of coils' and humidifier valves in a typical air-handling unit: Experimental impact assessment of indoor comfort and patterns of operating parameters under Mediterranean climatic conditions, Energies 15 (18) (2022) 6571, https://doi.org/10.3390/en15186571.
[41] A. Rosato, F. Guarino, M. El Youssef, M. Masullo, L. Maffei, Experimental assessment of ground-truth faults in a typical single-duct dual-fan air-handling unit under Mediterranean climatic conditions: Impact scenarios of sensors' offset and fans' failure, Energy Build. 275 (2022) 112492, https://doi.org/10.1016/j.enbuild.2022.112492.
[42] M. Halilovič, A. Kralj, J. Kurnitski, S. Domjan, A. Maček, S. Medved, Smart Readiness Indicator metric for building envelope structures, Energy Build. 350 (2025) 116677, https://doi.org/10.1016/j.enbuild.2025.116677.
[43] Ziehl-Abegg, RH31C-ZID technical datasheet. http://catalog.vseventilatory.ru/ziehl-abegg, 2025 (accessed 14 July 2025).
[44] Ziehl-Abegg, RH25C-6ID technical datasheet. http://catalog.vseventilatory.ru/ziehl-abegg, 2025 (accessed 14 July 2025).
[45] CAREL, Humidifiers technical datasheet. https://www.carel.com/documents/10191/0/2B030220621/92fca658-a251-49ee-9979-b8829fcba49f?version=1.0, 2025 (accessed 14 July 2025).
[46] AERMEC, Reversible air/water heat pump technical datasheet. https://download.aermec.com/docs/schede/ANL-021-203-HP_Y_UN50_03.pdf?r=14395, 2025 (accessed 14 July 2025).
[47] National Instruments, LabVIEW (Version 2019 SP1) [software], National Instruments, Austin, TX, USA, 2019.
[48] R. Mastrullo, A. Rosato, G.P. Vanoli, J.R. Thome, A methodology to select the experimental plant instrumentation based on an a priori analysis of measurement errors and instrumentation cost, Int. Commun. Heat Mass Transf. 35 (2008) 689–695, https://doi.org/10.1016/j.icheatmasstransfer.2008.02.006.
[49] Siemens, Duct sensors technical datasheet. https://www.downloads.siemens.com/download-center/Download.aspx?pos=download&fct=getasset&id1=24897, 2025 (accessed 14 July 2025).
[50] E+E Elektronik, EE210 outdoor sensor technical datasheet. https://www.epluse.com/fileadmin/data/product/ee210/datasheet_EE210_Outdoor.pdf, 2025 (accessed 14 July 2025).
[51] TSI, Q-Trak technical datasheet. https://tsi.com/getmedia/d2a8d1d1-7551-47fe-8a0f-3c14b09b494b/7575_QTrak_A4_UK_5001356-web?ext=.pdf, 2025 (accessed 14 July 2025).
[52] MEASUREIT, Sensors. https://shop.measureit.eu/sensori.html, 2025 (accessed 14 July 2025).
[53] Belimo, Energy valve technical datasheet. https://www.belimoseoul.com/data/medium/9d020b80b518dcf144d3cc8db59f777e.pdf, 2025 (accessed 14 July 2025).
[54] MEASUREIT, Voltage and current transducer datasheet. https://www.measureit.it/var/import/Attachment/DS_Mit_VI.pdf, 2025 (accessed 27 June 2025).
[55] R.J. Moffat, Describing the uncertainties in experimental results, Exp. Therm Fluid Sci. 1 (1988) 3–17, https://doi.org/10.1016/0894-1777(88)90043-X.
[56] Gestore Mercati Energetici (GME), Italian electricity market operator. https://www.mercatoelettrico.org/en-us/, 2025 (accessed 14 July 2025).
[57] G. Chicco, P. Mancarella, Assessment of the greenhouse gas emissions from cogeneration and trigeneration systems, Part i: Models Indicat. Energy 33 (2008) 410–417, https://doi.org/10.1016/j.energy.2007.10.006.
[58] F. Ceglia, E. Marrasso, C. Roselli, M. Sasso, Energy and environmental assessment of a biomass-based renewable energy community including photovoltaic and hydroelectric systems, Energy 282 (2023) 128348, https://doi.org/10.1016/j.energy.2023.128348.
[59] D.L.D. Harvey, A Handbook on Low-Energy buildings and District-Energy Systems: Fundamentals, Techniques and Examples, first ed., Routledge, London, 2012.
[60] Electricity Maps, Carbon intensity data for electricity generation. https://www.electricitymaps.com/, 2025 (accessed 14 July 2025).